Key Points:
- Magnetic and X-ray diffraction analyses on natural samples corroborate the efficiency of certain chemical extractions, such as dithionite
- The majority of iron in the oxalate extraction is not dissolved from magnetite, but instead comes from iron-bearing clays
- Recognition of the heterogeneity in chemical extraction efficiency and targeting is vital for studies of past and present iron cycling

Correspondence to:
S. P. Slotznick,
sslotz@dartmouth.edu

Unraveling the Mineralogical Complexity of Sediment Iron Speciation Using Sequential Extractions

S. P. Slotznick[1], E. A. Sperling[2], N. J. Tosca[3], A. J. Miller[2], K. E. Clayton[3], N. A. G. M. van Helmond[4], C. P. Slomp[4], and N. L. Swanson-Hysell[1]

[1]Department of Earth and Planetary Science, University of California, Berkeley, CA, USA, [2]Department of Geological Sciences, Stanford University, Stanford, CA, USA, [3]Department of Earth Sciences, University of Oxford, Oxford, UK, [4]Department of Earth Sciences-Geochemistry, Faculty of Geosciences, Utrecht University, Utrecht, Netherlands

Abstract Iron speciation is one of the most widely applied proxies used to reconstruct oxygen levels and redox conditions in past aqueous environments. The iron speciation proxy estimates proportions of different reactive iron species in fine-grained sedimentary rocks, which are mapped to redox conditions based on empirical calibrations from modern sediments. It is based on a standardized extraction technique of sequentially applying acetate, hydroxlamine-HCl, dithionite, and oxalate solutions to a powdered sample in order to dissolve iron phases and quantify the amount of iron carried by carbonates, "easily reducible" oxyhydroxides, ferric iron (oxyhydr)oxides, and magnetite, respectively. Although tested on pure minerals and mixtures, assessments of whether this sequential extraction process accurately dissolves the targeted minerals in natural sediments and sedimentary rocks are lacking. In our study, residues from each sequential extraction step were analyzed using rock magnetic and X-ray diffraction experiments to identify and quantify the iron-bearing minerals that were dissolved. The dithionite extraction robustly removes the targeted mineralogy as magnetic data show it to solubilize nearly all of the goethite. However, magnetic quantification of magnetite was orders of magnitude less than the iron measured in the oxalate extraction; X-ray diffraction data suggest that dissolution of iron-bearing clays, specifically berthierine/chamosite, could explain this disparity. Our data compilation shows higher values of iron from the oxalate extraction in Precambrian sedimentary rock samples, suggesting a significant temporal shift in iron cycling. Recognition of heterogeneity in chemical extraction efficiency and targeting is vital for holistic multiproxy interpretation of past oxygen levels and communication between disciplines.

Plain Language Summary Sequential chemical extractions, where a series of solutions are applied to a powdered rock sample to selectively dissolve certain phases, are heavily utilized throughout Earth Science research. These methodologies provide a tool for estimating different reactive forms of an element; understanding how these pools change over time in a given environment allows us to better understand cycling of the element by biological, chemical, and geologic processes on the Earth's surface. In this study, we focus on a sequential chemical extraction method that measures the element iron, the most abundant transition metal in Earth's crust. Although heavily utilized for understanding nutrient cycling and ancient oxygen levels, the method is largely untested using actual rock samples that contain a mixture of minerals of different shapes and sizes. Such tests are needed to evaluate whether the extractions are accurately and completely dissolving the targeted minerals. We utilized magnetic and X-ray diffraction methods that can sensitively measure iron minerals within natural samples. We found that some of the extractions worked as expected, but others did not, dissolving additional unexpected mineral types and/or slowly dissolving minerals across multiple extractions.

1. Introduction

Iron is the most abundant transition metal in the Earth's crust and is utilized by nearly all life. Due to its redox sensitivity as it cycles between +2 and +3 valence states, iron chemistry and mineralogy are frequently utilized to fingerprint metal mobility, nutrient cycling, and redox conditions in modern and ancient environments. Wet geochemical (sequential) extractions have dominated these efforts for the past 40 years, specifically, separating and measuring proportions of iron in distinct operationally defined pools (e.g., Berner, 1970; Tessier et al., 1979).

Iron speciation has become one of the most widely applied proxies for paleoredox and oxygen levels, redefining interpretations of redox conditions in the Precambrian and Paleozoic (Poulton & Canfield, 2011;

Sperling et al., 2015). Developing from work by Bob Berner and his students and colleagues at Yale, the proxy is based on a shelf-to-basin iron shuttling model (Lyons & Severmann, 2006; Raiswell & Canfield, 2012). The proxy has had several iterations (see Raiswell & Canfield, 2012 for history), but most recent studies rely on the geochemical sequential extraction methodology developed by Poulton and Canfield (2005). This method takes powdered sedimentary rock samples and measures different proportions of iron through three to four sequential extraction steps: (1) sodium acetate to target iron carbonates, (2) hydroxylamine-HCl for easily reducible iron oxides (typically skipped in analyses of ancient sedimentary rocks), (3) sodium dithionite for Fe^{3+} oxides, and (4) ammonium oxalate for magnetite ($Fe^{2+}Fe^{3+}_2O_4$). Separate extractions are used to measure the sulfide phases—both chromium reducible sulfides like pyrite (FeS_2) and acid volatile sulfides (AVS) like greigite ($Fe^{2+}Fe^{3+}_2S_4$) and pyrrhotite ($Fe_{1-x}S$ where $x = 0$ to 0.2). Total iron of a sample is quantified either by X-ray fluorescence or wet chemical methods such as inductively coupled plasma optical emissionspectrometry (ICP-OES) or flame atomic absorption spectroscopy. Although created to probe redox conditions of ancient sedimentary rocks, this extraction methodology has also been utilized to understand Holocene to modern sediments and modern (microbial) cycling of iron and other metals (e.g., Cai et al., 2018; Egger et al., 2016; von der Heyden et al., 2018) and the Poulton and Canfield (2005) methodology paper has been cited over 500 times.

The Poulton and Canfield (2005) methodology is operational and is not intended to define mineralogy, but it is linked to mineralogy through tests on standards and mixtures of pure minerals. Perfect selectivity is not possible as iron minerals display a range of reactivities depending on grain size, exact composition, crystallinity, and mineralogical associations (e.g., Raiswell et al., 1994), but researchers applying the method often use mineral-specific shorthand for the iron removed during each extraction (e.g., Fe_{mag} for iron removed during the oxalate step). However, the application of this iron speciation interpretation scheme to natural samples has led to a lingering debate about its accuracy and efficiency in diagenetically stabilized rocks (e.g., Raiswell et al., 2011; Reinhard et al., 2009; Reuschel et al., 2012) and in modern sediment samples (e.g., Bacon & Davidson, 2008; Egger et al., 2015; La Force & Fendorf, 2000) (also addressed in Raiswell et al., 2018). A few studies have paired iron speciation with other methods of identifying mineralogy, corroborating reports of issues with accuracy and/or suggesting the need for modification (e.g., Schröder et al., 2016; Slotznick, Swanson-Hysell, et al., 2018; *J* Sun et al., 2018). In this study, we use rock magnetic and spectroscopic techniques to characterize and quantify the minerals removed from natural samples after each extraction step. This approach provides a means to test whether the sequential extraction accurately dissolves the targeted iron-bearing minerals in natural sediments and sedimentary rocks and assess the potential for significant errors in determining iron pools within the iron speciation proxy.

2. Methods and Materials

Our approach was to characterize bulk powders as well as residues taken after each sequential extraction step, utilizing magnetic and spectroscopic techniques. The experiments were designed to independently identify and quantify the iron-bearing minerals that were dissolved by each step. In order to do this, we performed the sequential extraction procedure on three or four aliquots of the same powdered sample, removing one aliquot for analysis after each sequential extraction step. This approach means that for each sample we analyzed an untreated specimen, a specimen that underwent the acetate extraction, a specimen that underwent the acetate and dithionite extractions, and a specimen that underwent the acetate, dithionite, and oxalate extractions.

2.1. Sediment, Shale, and Siltstone Samples

Twenty natural rock and sediment samples were chosen for this study that span in age from the Holocene to the Mesoproterozoic (~1.5 Ga) (Table 1). Lithologically, all the samples are fine-grained siliciclastics—siltstones to shales to unlithified sediments. All samples selected had been previously characterized using either iron speciation or rock magnetic experiments (Dijkstra et al., 2016; Egger et al., 2016; Slotznick et al., 2019; Sperling et al., 2013; Sperling et al., 2015); these data were used to select for a diversity of total iron contents and iron extraction pools/mineralogy. Iron speciation analyses performed for this study demonstrate that the samples have different proportions of iron from each iron speciation extraction, leading to distinct paleoredox interpretations (Figure 1 and Table S1 in the supporting information).

Table 1
Sediments and Sedimentary Rock Samples Analyzed in This Study

Sample	Age	Formation	Location	Core or outcrop	Lithology	Ref.[a]
SBC-1[b]	Carboniferous	Glenshaw Fm., Conemaugh Group	Pennsylvania, USA	Outcrop	Shale	
SGR-1[b]	Eocene	Mahogany zone, Green River Fm.	USA	Outcrop	Shale	
GO130-286	Tonian	Fifteenmile Group	Yukon, Canada	Outcrop	Shale	1
MP-69.5	Cambrian	Wheeler Fm.	Utah, USA	Outcrop	Calcareous shale	2
RI-07-07A-92	Devonian	Canol Fm.	Yukon, Canada	Core	Shale	
15-TF-05-176	Silurian	Road River Group	Yukon, Canada	Outcrop	Calcareous shale	
15-TF-05-186	Silurian	Road River Group	Yukon, Canada	Outcrop	Shale	
AMB4	Ediacaran	Mall Bay Fm.	Newfoundland, Canada	Outcrop	Silty shale	
AMB6	Ediacaran	Mall Bay Fm.	Newfoundland, Canada	Outcrop	Silty shale	
F849-225	Ediacaran	Sheepbed Fm.	Yukon, Canada	Outcrop	Shale	3
BS13-10A	Calymmian	Lower Newland Fm.	Montana, USA	Outcrop	Dolomitic shale	4
GP12-1	Calymmian	Appekunny Fm., Mbr. 2	Montana, USA	Outcrop	Siltstone	4,5
GP12-8B	Calymmian	Prichard Fm./Appekunny Fm., Mbr. 4	Montana, USA	Outcrop	Muddy siltstone	4,5
T095-53	Calymmian	Upper Newland Fm.	Montana, USA	Core	Dolomitic shale	4,6
T095-408	Calymmian	Upper Newland Fm.	Montana, USA	Core	Sulfide ore	4
T112-334	Calymmian	Lower Newland Fm.	Montana, USA	Core	Shale	4,6
BLKS-1	Holocene	Black Sea Lake stage	Black Sea	Core	Pyritized black mud	7[c]
BLKS-2	Holocene	Black Sea Lake stage	Black Sea	Core	Gray mud	7[d]
BTCS-1	Holocene	Ancylus Lake stage	Baltic Sea	Core	Dark gray clay	8[e]
BTCS-2	Holocene	Baltic Ice Lake stage	Baltic Sea	Core	Gray/grayish brown clay	8[f]

[a]Reference for prior iron speciation or magnetic studies on the sample. All iron speciation data (except Fe_T and Fe_{CRS}) were remeasured for this study. (1) Sperling et al. (2013); (2) Sperling et al. (2015); (3) Johnston et al. (2013); (4) Slotznick et al. (2019); (5) Slotznick et al. (2016); (6) Slotznick et al. (2015); (7) Egger et al. (2016); (8) Dijkstra et al. (2016). [b]USGS Standard. [c]PHOXY4 GC—213–243 cm bsf. [d]PHOXY4 GC—478–508 cm bsf. [e]IODP63—Sample 30; Core 21, Section 1—40.73 m bsf. [f]IODP63—Sample 43; Core 33, Section 1—65.15 m bsf.

2.2. Sequential Chemical Extractions

Iron sequential extractions were performed in two different laboratories using the established protocols (Poulton & Canfield, 2005): 1M sodium acetate at pH 4.5 for 48 hr at 50 °C, 1-M hydroxylamine-HCl in 25% v/v acetic acid for 48 hr (on Holocene/modern samples), sodium dithionite solution (0.29 M) buffered to pH 4.8 with 0.35-M acetic acid/0.2-M sodium citrate for 2 hr, and 0.2-M ammonium oxalate/0.17-M oxalic acid solution at pH 3.2 for 6 hr. At Stanford, where analyses of ancient shales and siltstones were performed,
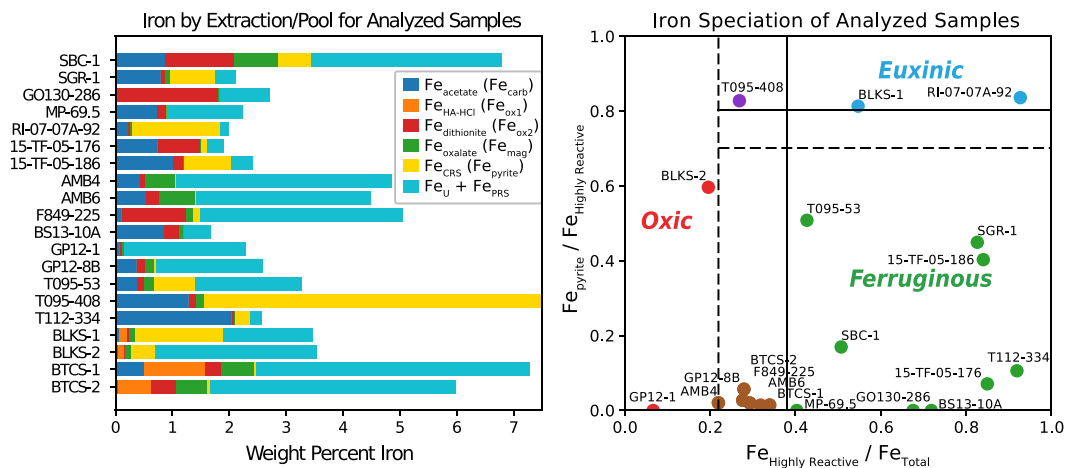

Figure 1. Iron speciation of the 20 samples shown with details of the iron extracted at each step on the left and plotted within the iron speciation proxy framework for paleoredox on the right. The pools in the bar plot are colored by the chemical extraction with the more commonly used abbreviations signaling the targeted mineralogy shown in parentheses in the legend (Poulton & Canfield, 2005). Abbreviations: carb = carbonate, HA-HCl = hydroxylamine-HCl, ox1 = easily reducible oxides, ox2 = reducible oxides, mag = magnetite, CRS = chromium reducible sulfur, U = unreactive, PRS = poorly reactive sheet silicates, $Fe_{Highly\ Reactive}$ = $Fe_{acetate} + Fe_{HA-HCl} + Fe_{dithionite} + Fe_{oxalate} + Fe_{CRS}$. Note: T095-408 is off scale on the bar plot—see Tables 1 and S1 for additional information and data on all samples.

iron removed during these extractions was measured spectrophotometrically using the ferrozine method of Stookey (1970) with color development allowed to proceed overnight. Samples were processed alongside four in-house standards, and results for these standards matched previous analyses, including those in other labs (Kunzmann et al., 2015; Sperling et al., 2015). Previous analyses of these standards have demonstrated a standard error of the mean of <5% for all iron pools greater than 0.3 wt% (see table S7 of Sperling et al., 2015, for full description of error estimates for many of these standards). Precision for very low weight percent iron pools is lower, but error on such samples will have negligible impact on iron speciation ratios in samples with sufficiently high total iron. Due in part to such errors, case studies suggest that samples with very low weight percent total iron should not be used for iron speciation paleoredox interpretations (Raiswell et al., 2018). Some samples used in this study had been analyzed dozens of times before at Stanford; individual means and standard deviations for each extraction are shown in Figure S1. Iron in pyrite was analyzed through a 2-hr boiling acidic chromous chloride extraction following the protocol of Canfield et al. (1986), with extracted sulfide (called CRS for chromium reducible sulfur) trapped and measured gravimetrically. Based on replicates of an in-house Silurian shale standard (J1518-273.5-B), percent standard deviation for CRS is 8.7% and percent standard error of the mean is <1%, consistent with precision on previous shale standards (Sperling et al., 2013; Sperling et al., 2015). Total iron and manganese abundances were measured at Bureau Veritas Minerals, Vancouver, Canada. Samples were digested using a standard four-acid digestion or in a lithium borate fusion and measured using ICP-OES. Samples were analyzed alongside blind aliquots of U.S. Geological Survey standards SBC-1 and SGR-1. While we were not able to establish precision for these standards at this lab, single analyses for total iron were within 4% and 7% of published values, respectively, and a Bureau Veritas in-house standard had a percent standard deviation of 1.3% for iron.

At Utrecht University, where analyses of Holocene and modern sediments from the Baltic Sea and the Black Sea were performed, iron removed during the Poulton and Canfield (2005) extraction under oxygen-free conditions was measured spectrophotometrically using the 1,10-phenanthroline method (APHA, 2005), with color development allowed to proceed overnight. Relative errors were generally less than 10% and often less than 5%, based on duplicates, triplicates, and in-house standards. For samples from the Baltic Sea, iron carried by sedimentary iron-sulfur phases was determined using the procedure of Burton et al. (2008). Briefly, 0.5 g of sediment was extracted under oxygen-free conditions using (1) 10-ml 6-M HCl and 2-ml 0.1-M ascorbic acid to dissolve AVS (assumed to represent Fe monosulfides); the released H_2S was trapped in a tube filled with 7 ml of an alkaline zinc acetate solution (24 hr); (2) 10-ml acidic chromium (II)chloride to dissolve CRS (assumed to represent pyrite); the released H_2S was trapped with 7 ml of an alkaline zinc acetate solution (48 hr). For both methods, the amount of sulfur in the zinc sulfide precipitates was determined by iodometric titration (APHA, 2005). For samples from the Black Sea, pyrite-iron was determined by sequential extraction using a nitric acid extraction, concentrated HNO_3 for 2 hr (Claff et al., 2010), although it will be grouped with Fe_{CRS} in this paper for simplicity. Average analytical uncertainty, based on duplicates and triplicates, was <6% for AVS and CRS. Total sedimentary Fe contents were determined with ICP-OES after digestion with a mixture of $HClO_4$, HNO_3, and HF (Van Helmond et al., 2018). The relative error was generally less than 3% based on duplicates, triplicates, and in-house standards.

2.3. Rock Magnetic Methods

Nondestructive bulk rock magnetic experiments were performed to observe fundamental magnetic properties that can distinguish between different magnetic minerals and provide information about their abundance (Table S2). All minerals have magnetic properties, but in many phases, the magnetism is very weak even when exposed to a magnetic field. Paramagnetic minerals contain atoms or ions with unpaired electrons (such as iron) that result in a magnetization when an external magnetic field is applied; however, when the field is removed, their magnetization returns to zero. Ferromagnetic minerals (sensu lato) are minerals with specific crystal structures that allow a magnetization to be retained once a magnetic field is removed, often called a remanent magnetization or remanence. For the magnetic experiments, bulk powders and residues from the sequential extractions were individually packed into gelatin capsules, along with quartz wool, and ranged in mass from 40 to 250 mg. The four modern sediment samples and their residues were packed inside of an anoxic glovebox. They were transferred within plastic vials tubes filled with nitrogen directly to a vacuumed system for low-temperature magnetic measurements at the Institute for Rock Magnetism at the

University of Minnesota. Room temperature magnetic measurements were conducted immediately afterward in Minnesota and over the next 3 weeks at UC Berkeley. Although stored short term in plastic tubes with a nitrogen atmosphere and long term in an anoxic glovebox, the samples were exposed to air for approximately 10 days over the course of these measurements. For specimens that underwent chemical treatment(s), all magnetic measurements are mass normalized to initial mass of the powder pretreatment except for the saturation magnetization (M_s) and remanent saturation magnetization (M_{rs}) measurements used for quantification.

At the Institute for Rock Magnetism, hysteresis loops and DC demagnetization experiments were conducted on all specimens at room temperature using a Princeton Measurements Vibrating Sample Magnetometer (VSM). These experiments enabled the calculation of M_s as well as determination of the coercivity spectrum for each sample. To develop coercivity spectra with lower noise than on the VSM, alternating field (AF) demagnetization of isothermal remanent magnetization experiments were conducted using the UC Berkeley Paleomagnetism Laboratory's 2G Enterprises superconducting quantum interference device magnetometer with RAPID automatic sample handling and software (Kirschvink et al., 2008). Coercivity is an inherent property of ferromagnetic minerals (e.g., Peters & Dekkers, 2003), and coercivity spectra of specimens with complex mineral assemblages can be used to identify different mineral phases and their progressive loss through sequential chemical treatments.

In addition to coercivity, many magnetic minerals can be identified by their unique low-temperature transitions. Using a Quantum Designs Magnetic Property Measurement System at the Institute for Rock Magnetism, rock magnetic experiments were performed on 71 out of 81 specimens to corroborate ferromagnetic mineral identifications, identify additional phases which become ferromagnetic at low-temperature, and provide another method for investigating mineralogical changes between sequential extraction steps. In these experiments, each sample was cooled in a 2.5 T field from 300 to 10 K, then the field was turned off, and remanence measurements were made upon warming (field-cooled low-temperature saturation isothermal remanent magnetization, FC LTSIRM). Next, the sample was cooled to 10 K with no applied field, at 10 K it was pulsed with a 2.5 T field, and then remanence measurements were made upon warming (zero-field-cooled low-temperature saturation isothermal remanent magnetization, ZFC LTSIRM). Finally, the sample was pulsed with a 2.5 T field at 300 K before cooling to 10 K and warming back to 300 K during which remanence measurements were made (room temperature saturation isothermal remanent magnetization, RTSIRM, cooling and warming).

During static AF demagnetization, gyroremanent magnetization (GRM) can be acquired by anisotropic samples in a direction oriented orthogonal to that of the AF (Stephenson, 1993). Many magnetic minerals can acquire GRM at high applied fields, but greigite acquires a particularly large GRM which can be used for identification purposes (e.g., Hu et al., 1998; Hu et al., 2002). We tested for GRM acquisition in 11 of the samples using the Berkeley magnetometer following the protocol of Garrick-Bethell et al. (2009) and Tikoo et al. (2012). As there was no natural remanent magnetization in our powders and residues, samples were given an angled isothermal remanent magnetization of ~1.5 T. In the five cases where the bulk powder specimen acquired some GRM, additional specimen(s) were run to determine if the signal remained after chemical treatment(s).

Magnetic quantification of magnetite abundance was possible for specimens by dividing the measured M_s by that for pure magnetite (Klein et al., 2014; Slotznick et al., 2019). A range of M_s values for magnetite have been reported in the literature from 73 to 92 Am^2/kg (e.g., Aharoni et al., 1962; Bate, 1980; Dunlop, 1986; Heider et al., 1996; Pauthenet, 1950; Peters & Dekkers, 2003; Smit & Wijn, 1959), and we will follow the convention that the highest, 92 Am^2/kg, is closest to the true value. The quantification calculation assumes that magnetite is the only ferromagnetic mineral in the sample. It is therefore a maximum value and could not be performed on samples and specimens with appreciable quantities of other ferromagnetic minerals. For example, some samples contained maghemite (γ-Fe$_2$O$_3$); however, this should be (and was) solubilized by the dithionite extraction and therefore, quantification could be performed on these samples in specimens after the dithionite step.

Magnetic quantification was also performed for monoclinic pyrrhotite in Sample GP12-8B. If there was trace magnetite mixed with the pyrrhotite, the M_s would be affected; thus, M_{rs} was used instead of M_s as it is less

sensitive to magnetite abundance within samples as the two minerals have more similar M_{rs} values (Dekkers, 1988; Peters & Dekkers, 2003). A range of M_{rs} for pyrrhotite have been reported in the literature ranging from 1.5 to 9.3 Am^2/kg based on grainsize and slight differences in chemical formula with an average of 5.0 Am^2/kg (Clark, 1984; Dekkers, 1988; Peters & Dekkers, 2003). The quantification also assumes that pyrrhotite is the only ferromagnetic mineral in the sample and thus should be treated as a maximum; as a result, we use the lowest M_{rs} reported in our calculations.

Goethite has a characteristic large difference between the FC and ZFC LTSIRM data with much greater remanence acquired during the FC experiment as well as large decreases in remanence upon warming (Dekkers, 1989a; Guyodo et al., 2003 ; Liu et al., 2006). Qualitative approximation of goethite abundance was performed using these experimental results (such as in Kars et al., 2015; Figure S19); however, several factors prevented us from performing absolute quantification. First, goethite has a large range of measured M_s and M_{rs} spanning an order of magnitude even at room temperature (Dekkers, 1989b; Peters & Dekkers, 2003), which are much lower than other ferromagnetic phases making quantification in mixed phase natural samples difficult. Second, the 1.4 T high field used on the VSM and the 2.5 T on the Magnetic Property Measurement System will not fully magnetize the goethite present in the samples, as goethite has been shown to remain unsaturated above these fields, even up to >57 T (Rochette et al., 2005). Third, goethite has a wide range of blocking temperatures based on grain size, composition, and crystallinity, which can be below room temperature; therefore, high fields applied at room temperature would not saturate these (subset of) particles either (Guyodo et al., 2003; Liu et al., 2006). Methods such as Mössbauer and X-ray absorption spectroscopy have the potential to more robustly quantify goethite weight percent and could be utilized in future work.

2.4. X-ray Diffraction Methods

Powder X-ray diffraction (XRD) measurements were made on all of the samples at the University of Oxford. Each specimen was analyzed using two different approaches on a PANalytical Empyrean Series 2 powder diffractometer with PIXcel1D detector, operating at 40 kV and 40 mA, and utilizing a Co Kα source. Both analyses were performed using powder that was deposited on a zero-background single crystal silicon substrate and mounted on spinning sample stage during analysis (rotating at 10 revolutions per minute). A bulk analysis from 5° to 80° two theta is used to identify major minerals present. This analysis is done by identifying statistically meaningful peaks and matching their intensity and position with minerals using the International Center for Diffraction Data Powder Diffraction File 4+ database of mineral standards. Quantification of minerals identified in the bulk analysis is performed using the reference intensity ratio method (Snyder & Bish, 1989) and scale factors published with mineral standards in the International Center for Diffraction Data PDF-4+ database.

A second analysis is run on each specimen to further constrain clay mineralogy, by focusing on the high-angle region of the diffraction pattern between 69° and 75° two theta. In this region, clay minerals exhibit diagnostic 060 reflections, which directly correspond to octahedral layer composition (but are insensitive to structural defects), therefore allowing clay mineral speciation at the family level (i.e., Fe-rich chlorites and/or serpentine (berthierine), Mg-rich chlorites, Fe-rich dioctahedral 2:1 clays and micas, Al-rich dioctahedral 2:1 clays and micas, and kaolinites) (Srodon et al., 2001). Peaks were deconvolved using Panalytical HighScore peak fitting software and then assigned to mineralogy. Abundances of clay determined by this method scale linearly with peak area in this part of the pattern, so quantification is possible by first determining relative abundances with respect to quartz as an internal standard and then multiplying these abundances by the total amount of quartz determined through the bulk analysis.

3. Results and Mineralogy Interpretation

Based on the results of the rock magnetic experiments, ferromagnetic minerals were identified for the bulk untreated samples. The minerals identified through these experiments were siderite ($FeCO_3$), ferrihydrite ($Fe_2O_3 \cdot 0.5(H_2O)$), goethite (α-FeO(OH)), hematite (Fe_2O_3), maghemite, (oxidized) magnetite, pyrrhotite, and greigite. Magnetic parameters were also used to approximate the abundance of paramagnetic minerals in the sample (Richter & van der Pluijm, 1994) (Table S1 and Figure S18). Comparison of low-temperature experiments and coercivity spectra on specimens after each extraction experiment allowed
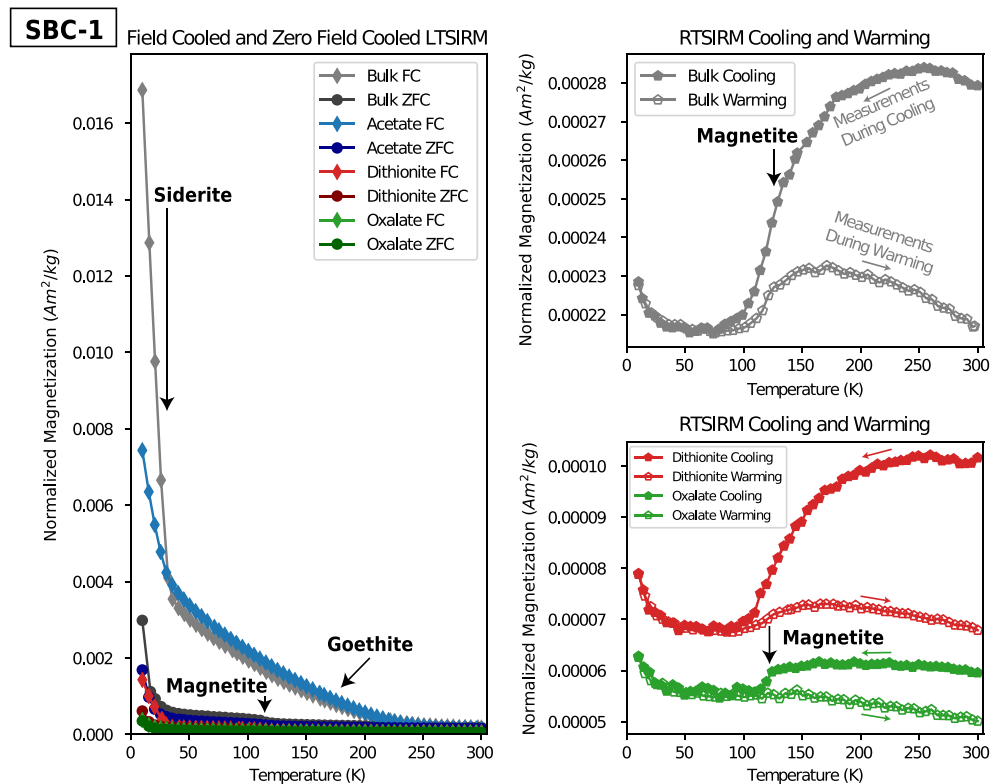
Figure 2. Low-temperature magnetic analyses after each extraction for sample SBC-1 (Carboniferous Brush Creek Shale, Glenshaw Formation, USA). The bulk curves represent the untreated powdered rock, acetate denotes the specimen that only underwent the acetate extraction, dithionite the specimen that underwent acetate + dithionite extractions, and oxalate the specimen that underwent acetate + dithionite + oxalate extractions. For this sample, the data suggest that the sample contains siderite, magnetite, and goethite based on their diagnostic low-temperature transitions (annotated). The acetate step dissolved much of the siderite as well as some of the magnetite (also visible in the coercivity spectra Figure S13a.) The dithionite extraction showed a continued dissolution of siderite and magnetite as well as almost complete loss of goethite. The oxalate extraction solubilized a small amount of remaining siderite and magnetite. Abbreviations: LTSIRM = low-temperature saturation isothermal remanent magnetization, FC = field cooled, ZFC = zero-field cooled, RTSIRM = room-temperature saturation isothermal remanent magnetization.

for a qualitative assessment of the main effect of each extraction on the magnetic mineralogy of a given sample (Figures 2–8 and S2–S15). Quantitative estimates for the mineral magnetite were made by comparing magnetic quantification of the phase to the amount of iron extracted during the oxalate extraction (Figure 9).

XRD data were analyzed to identify major minerals including small amounts of the iron-bearing minerals pyrite, jarosite, magnetite, and ferric iron oxides (Table S3). Phases of varying composition known to contain iron such as calcite, dolomite/ankerite, and clays were also identified. A separate clay mineralogy analysis allowed for semiquantitative measurements of the distinct iron-bearing clays within the samples (Figure 10 and Table S3). These quantifications provided a tool for detecting dissolution of minerals after each extraction. Both the magnetic and XRD data contribute to the interpretations of the mineral phases extracted by each sequential step below.

3.1. Acetate Extraction

The acetate extraction is used to target iron contained within carbonates, which could include siderite and ankerite (Ca (Fe,Mg,Mn)$(CO_3)_2$) as well as Fe-bearing dolomite (CaMg $(CO_3)_2$), calcite ($CaCO_3$), and rhodochrosite ($MnCO_3$). Of these minerals, magnetic methods are only able to detect siderite, which can be identified in low-temperature experiments due to its Néel temperature of 37 K and characteristic behavior of the FC LTSIRM values being much greater than those in the ZFC LTSIRM experiment (Frederichs et al., 2003; Housen et al., 1996). Magnetic behavior consistent with siderite was noted in five of the samples (SBC-1, SGR-1, 15-TF-05-186, BS13-10A, and F849-225), but the mineral dominates the LTSIRM warming curve
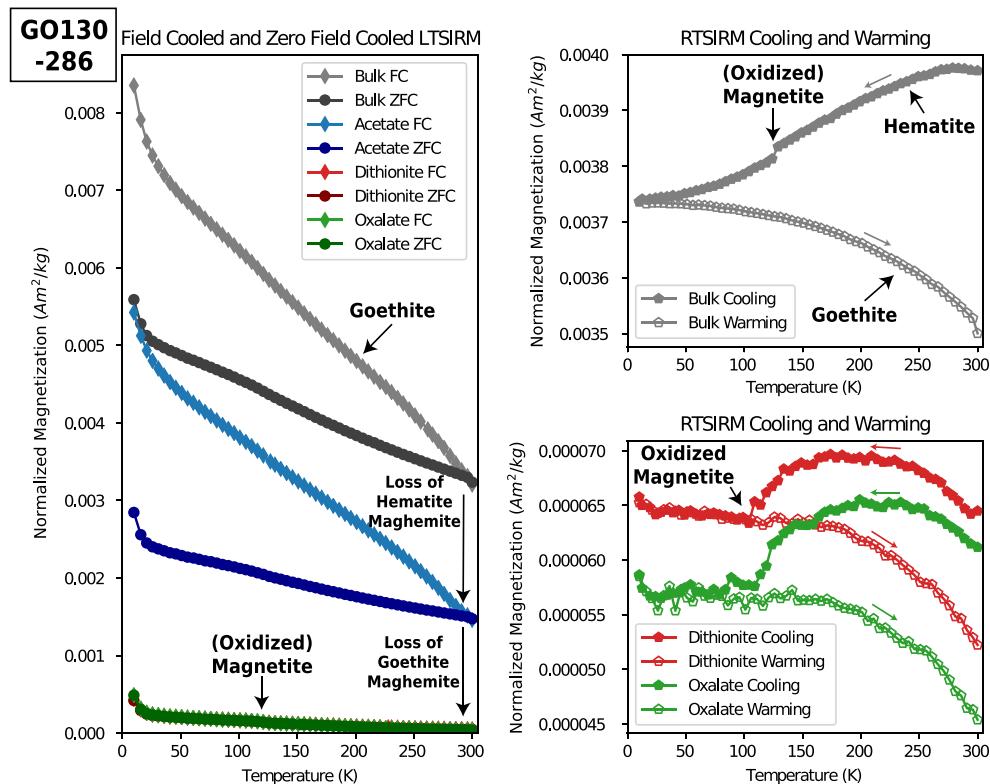
Figure 3. Magnetic analyses after each extraction for sample GO130-286 (Tonian Fifteenmile Group, Canada) suggest that the sample contains goethite and partially oxidized magnetite based on their low-temperature behavior (annotated). A high-coercivity phase with no low-temperature transitions except a decrease in RTSIRM during cooling is also noted and suggested to be hematite (see Figure S13b for coercivity spectra). Well shown in the coercivity spectra, the acetate step dissolved this high-coercivity phase and a low- to moderate-coercivity phase suggested to be maghemite or oxidized magnetite. The dithionite extraction effectively solubilized goethite and much of the maghemite/partially oxidized magnetite. Very little change is observed associated with the oxalate step. See Figure 2 caption for abbreviations.

behavior in the first four samples suggesting that it is relatively abundant compared to other ferromagnetic phases (Figures 2, S2, S6, and S9). These four samples showed large amounts of iron extracted during the acetate extraction (0.88 wt%, 0.80 wt%, 1.01 wt%, and 0.86 wt%), but other samples with similarly large amounts (>0.7 wt%) did not contain siderite suggesting the presence of iron in paramagnetic carbonate phases (evaluated in Figure S18). Our ability to evaluate the efficiency of this extraction is somewhat limited using magnetic techniques.

XRD analyses were able to measure the percentage of calcite and dolomite/ankerite within samples. However, the percentage of (trace) iron in these phases could not be determined, making inferences to the iron from acetate extraction indirect. Eight samples contained measurable calcite or dolomite/ankerite; four of these samples have low-temperature magnetic data that were interpreted here as indicative of siderite. All or almost all (below detection levels) of the calcite and dolomite was solubilized in these samples during the acetate extraction (Table S3). The only exception is the pyrite-ore sample (T095-408) suggesting mineral assemblage and association could affect dissolution of carbonates via acetate. Overall, based on XRD and magnetic measurements, the acetate extraction effectively targeted calcite, dolomite, ankerite, and siderite when they were present in the sample (e.g., SBC-1 and SGR-1; Figures 2 and S2). However, not all of the siderite was dissolved during this step for siderite-rich samples, as noted in other studies (Raiswell et al., 2011; Reinhard et al., 2009; Schröder et al., 2016).

In addition to siderite, other ferromagnetic minerals were noticeably dissolved during the acetate extraction demonstrating that the extraction solubilizes minerals not typically considered to be targeted by the step. Half of the samples showed a loss of room temperature remanent magnetization and dissolution of a high-coercivity phase tentatively interpreted to be the mineral hematite (e.g., GO130-286; Figures 3 and
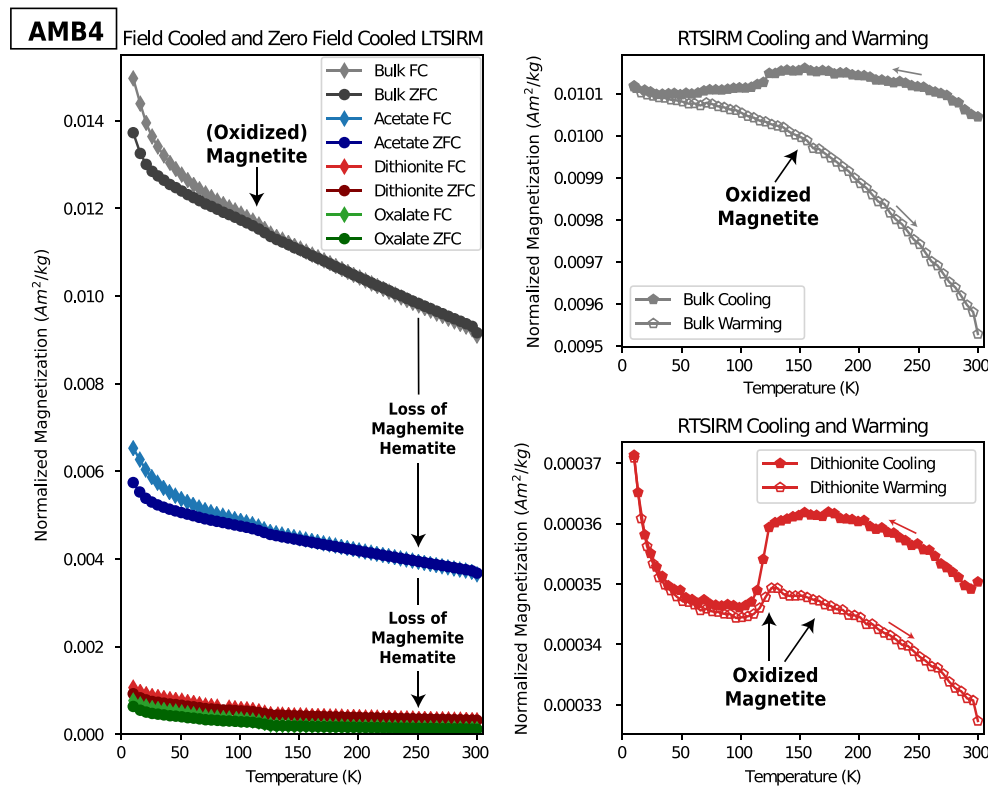
Figure 4. Magnetic analyses after each extraction for sample AMB4 (Ediacaran Mall Bay Formation, Canada) suggest that the sample contains (oxidized) magnetite based on its low-temperature behavior (annotated). The acetate extraction resulted a sharp drop in room-temperature magnetization. Based on the coercivity spectra (Figure S13c), this is due to the dissolution of a high-coercivity phase and a low- to moderate-coercivity phase with no low-temperature transitions suggested to be hematite and maghemite respectively, although greigite is also a possibility (see gyroremanent magnetization Figure S16). Continued dissolution of these two phases occurred during the dithionite extraction. The oxalate extraction noticeably further solubilized the high-coercivity phase (suggested to be hematite). See Figure 2 caption for abbreviations.

S13b). These samples did not have noticeable low-temperature transitions (the Morin transition, a magnetic transition at ~250 K (Morin, 1950; *J* Wang et al., 2015) or others), so this identification is tentative. Due to the remanent coercivity on the lower end of hematite's range, we suggest that this hematite is either very fine grained (<1 μm) or very large grained (>50 μm) (Özdemir & Dunlop, 2014; Peters & Dekkers, 2003). Nanophase hematite has been shown to form in diagenetic processes either during early diagenesis through aging of ferrihydrite or through secondary diagenetic processes repartitioning iron, for example from iron-bearing carbonates and silicates (Jiang et al., 2015; Swanson-Hysell et al., 2019; Walker et al., 1981; Weil & Van der Voo, 2002).

In addition to hematite, maghemite appears to have been dissolved during the acetate extraction (e.g., AMB4; Figures 4 and S13c). Maghemite does not contain a diagnostic low-temperature transition and has reversible RTSIRM curves upon cooling and warming. As a result, it can be difficult to identify unambiguously in multimineral natural samples. We interpreted its presence on the basis of its relatively low coercivity and loss of magnetization/coercivity peak height at room temperature between extractions (Özdemir & Dunlop, 2010; Peters & Dekkers, 2003); mineralogical interpretations other than maghemite could be valid for these properties. Maghemite was noted in five samples (GO130-286, MP-69.5, AMB4, AMB6, and BLKS-1) always with hematite or oxidized magnetite suggesting it results from oxidizing reactions during either protolith weathering, deposition, diagenesis, or modern weathering. In the first four listed samples interpreted to contain significant amounts of maghemite, approximately half of it was dissolved during the acetate extraction.

The original iron speciation methodology noted that AVS were also quantitatively solubilized during the acetate extraction (Poulton & Canfield, 2005). As with these other extractions, AVS are operationally
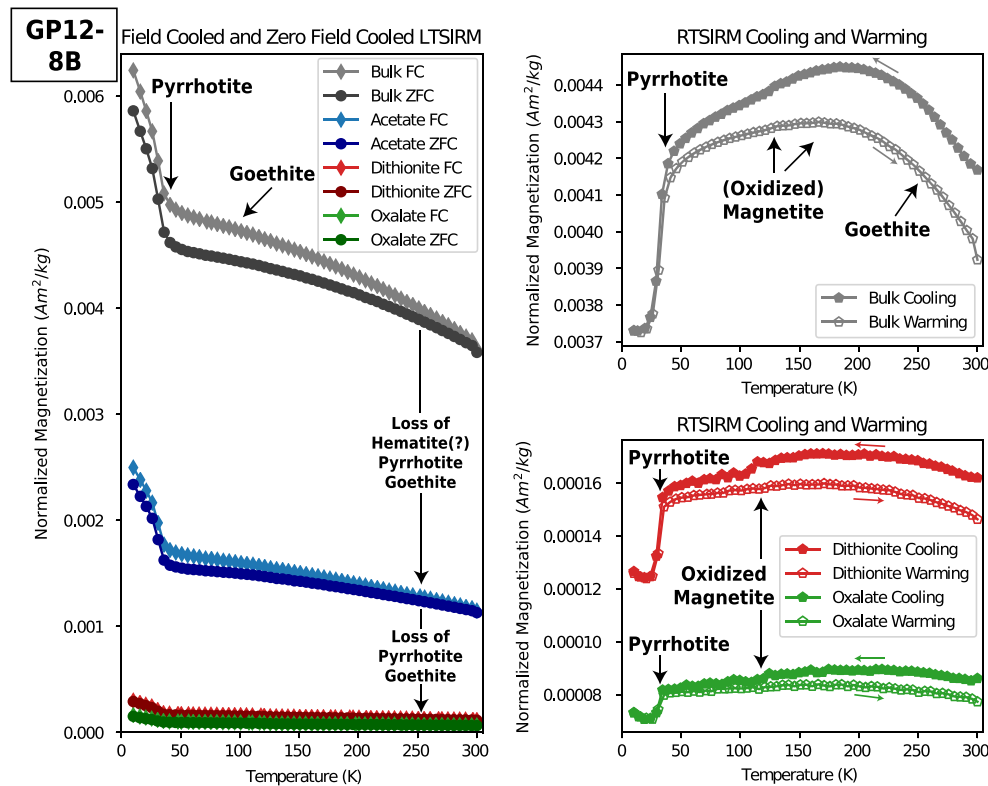
Figure 5. Magnetic analyses after each extraction for sample GP12-8B (Calymmian Prichard Formation/Appekunny Formation, Belt Supergroup, USA) suggest that the sample predominantly contains monoclinic pyrrhotite as well as minor oxidized magnetite and goethite based on its low-temperature behavior (annotated). A high-coercivity phase with no discernable low-temperature transition is also observed and interpreted to be hematite (Figure S12b). The acetate extraction dissolved most of this high-coercivity phase as well as some pyrrhotite and goethite. The dithionite extraction effectively solubilized the remainder of these two phases although a small amount of pyrrhotite remained and was slightly dissolved during the oxalate extraction. See Figure 2 caption for abbreviations.

defined and include amorphous Fe-S, mackinawite $((Fe,Ni)_{1 + x}S$ where $x = 0$ to 0.11), greigite, and pyrrhotite (Cornwell & Morse, 1987; Praharaj & Fortin, 2004). Iron speciation analyses on natural rock samples showed that the acetate extractions likely do not completely extract all the AVS/pyrrhotite especially in AVS-rich samples (Poulton et al., 2010; Reuschel et al., 2012). Our analyses on one sample with abundant monoclinic pyrrhotite (GP12-8B, magnetically quantified as 0.27 wt%) confirm these results with mineralogical rigor and show that approximately half of the pyrrhotite is dissolved in the acetate step (Figures 5 and S12b). Pyrrhotite was identified by its classic Besnus transition at 32 K (Besnus & Meyer, 1964; Rochette et al., 1990), and its presence was also suggested by moderate coercivity values above those typical for magnetite. Hexagonal (3T) pyrrhotite does not show the Besnus transition, and its room-temperature magnetic properties are poorly understood (Horng & Roberts, 2018); it could be present, but unidentified, in other samples within the suite.

Considering other AVS minerals, two samples of modern sediment contained greigite and this mineral may also be present in lower abundances in four shales formed during the Eocene to Ediacaran periods. Greigite is difficult to identify magnetically due to its lack of low-temperature transitions and coercivity range that overlaps with the ranges for magnetite and pyrrhotite (e.g., RI-07-07A-92, Figure S4). However, the acquisition of large GRM in greigite-bearing rocks (e.g., Hu et al., 1998; Hu et al., 2002) was used to confirm the mineral's presence in the two Holocene Black Sea samples (BLKS-1 and BLKS-2) and rule out its presence in other samples (Figures S16 and S17). Greigite is primarily extracted during the acetate extraction in these samples, but in the sediment sample with the largest abundance (BLKS-2), not all greigite was solubilized and it continued to be extracted in later sequential chemical steps (Figures 6 and S15a).

Overall, while the acetate extraction effectively targets most carbonate phases, it only partially dissolves the iron-carbonate siderite. The extraction partially dissolves monoclinic pyrrhotite and greigite when present in
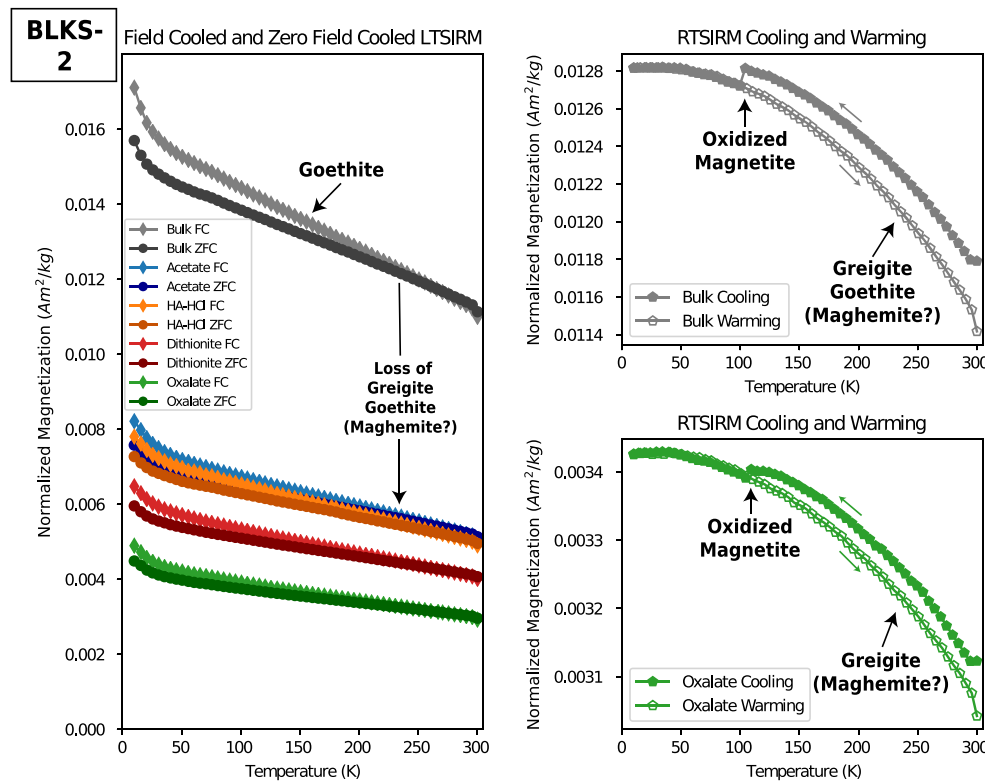
Figure 6. Magnetic analyses after each extraction for sample BLKS-2 (Holocene Black Sea sediment) suggest that the sample contains minor oxidized magnetite and goethite based on its low-temperature behavior (annotated). A moderate- to high-coercivity phase with no low-temperature transition other than linearly increasing RTSIRM during cooling dominates the sample (Figure S15a) and is interpreted to be greigite based on its large gyroremanent magnetization (Figure S16); minor maghemite (identified in the other Black Sea sample; Figure S14) could also be present. Greigite and goethite are primarily dissolved during the acetate extraction. Very little change in ferromagnetic phases is associated with the hydroxylamine-HCl (HA-HCl) extraction. During the dithionite extraction, the coercivity spectra do not show significant greigite dissolution, but a loss of magnetization in the low-temperature experiments suggests otherwise. The oxalate extraction solubilized some greigite as well. See Figure 2 caption for additional abbreviations.

abundance. The acetate extraction also appears to partially dissolve nontargeted iron oxides tentatively identified as maghemite and fine-grained hematite.

3.2. Hydroxylamine-HCl Extraction

The hydroxylamine-HCl extraction is applied to target "easily reducible" iron oxides like ferrihydrite and lepidocrocite. Due to the instability of these minerals on geologic time scales, analyses on pre-Quaternary sedimentary rocks usually do not include this extraction step due to very low abundances; if present, these phases will be extracted in the dithionite extraction. Therefore, hydroxylamine-HCl extractions were only applied to the four sediment samples from the Holocene epoch.

Ferrihydrite and lepidocrocite both can be probed using magnetic methods. Many studies have highlighted the wide range of magnetic properties for ferrihydrite depending on its structure, purity, grain-size, and ordering (Berquó et al., 2007; Guyodo et al., 2006; Michel et al., 2010; X Wang et al., 2016; Zergenyi et al., 2000). However, data show that remanent magnetization has a sharp decrease upon warming in both FC and ZFC LTSIRM experiments between 33 and 80 K—interpreted to be related to the blocking temperature. Lepidocrocite also shows a similar sharp drop in remanence in FC and ZFC LTSIRM experiments below 30 to 75 K, interpreted to be the Néel temperature (Guyodo et al., 2016; Hirt et al., 2002; Till et al., 2014). Unfortunately, in natural samples with complex mixtures of minerals, it can be difficult to distinguish these phases from superparamagnetic minerals such as nanophase hematite or goethite (e.g., Guyodo et al., 2003).

Two samples had sharp decreases in magnetic remanence during the FC and ZFC LTSIRM experiments that were interpreted to indicate ferrihydrite or lepidocrocite (BTCS-1 and RI-07-07A-92; Figures 7 and S4). In both samples, the acetate extraction dissolved a portion of the iron oxides ranging from ~25% to 75% of
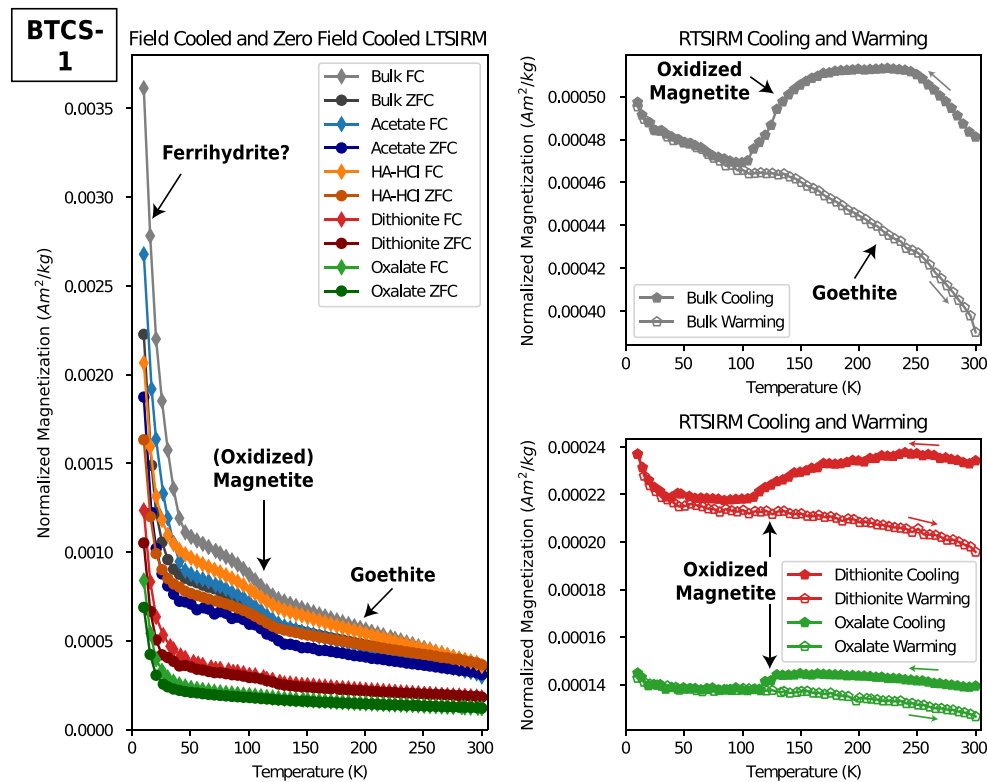
Figure 7. Magnetic analyses after each extraction for sample BTCS-1 (Holocene Baltic Sea, Ancylus Lake Stage sediment) suggest that the sample contains partially oxidized magnetite, ferrihydrite (or lepidocrocite), and goethite based on its low-temperature behavior (annotated). The acetate step dissolved some of the tentatively identified ferrihydrite and the goethite. The hydroxylamine-HCl (HA-HCl) extraction continued dissolution of the ferrihydrite and slightly solubilized oxidized magnetite. The HA-HCl specimen has a slight stronger magnetization than the "previous" acetate specimen; we interpret that this is due to specimen differences from either the subsampling of initial powder, extraction protocol, and packing for magnetic analyses. During the dithionite extraction, goethite was completely solubilized as was the remainder of the ferrihydrite; most of the loss of oxidized magnetite also occurred during this step (also apparent in the coercivity spectra, Figure S15b). In the oxalate extraction, some of the remaining oxidized magnetite is solubilized. See Figure 2 caption for abbreviations.

the total amount. One of these samples was a Holocene sediment to which hydroxylamine-HCl was applied resulting in a decrease in ferrihydrite/lepidocrocite abundance (BTCS-1; Figure 7). However, this decrease was similar in magnitude to the loss observed from the acetate extraction, which was observed in both samples. In both samples, the subsequent dithionite extraction fully removed the remainder of these oxide phases. Although only two samples, it appears that the hydroxylamine-HCl extraction did target easily reducible iron oxides when present, but these phases also dissolved in earlier and later steps.

More broadly, the hydroxylamine-HCl extraction only minimally dissolved other ferromagnetic phases. A slight decrease in oxidized magnetite was noted (BTCS-1 and BTCS-2; Figures 7, 8, and S15) and some maghemite was also dissolved (BLKS-1; Figure S12). Pure maghemite was not analyzed in the Poulton and Canfield (2005) sequential extraction methodology, and it is rarely analyzed in experiments on aqueous reactivity (e.g., Poulton et al., 2004); maghemite might be considered an easily reducible iron oxide based on its dissolution/reactivity in nature (e.g., Yamazaki & Solheid, 2011) or could be grouped with the other Fe^{3+} iron (oxyhydr)oxides or magnetite based on its chemistry and structure.

3.3. Dithionite Extraction

The dithionite extraction is used to target Fe^{3+} oxides and oxyhydroxides, specifically goethite, akaganeite, and hematite (Poulton & Canfield, 2005). Goethite and hematite have high coercivities with hematite typically having remanent coercivities >100 mT and goethite typically >1,000 mT (Peters & Dekkers, 2003). These high coercivity values for goethite are above those reached in the coercivity spectra measured here, and its identification was based on low-temperature magnetic experiments. Goethite can be identified by
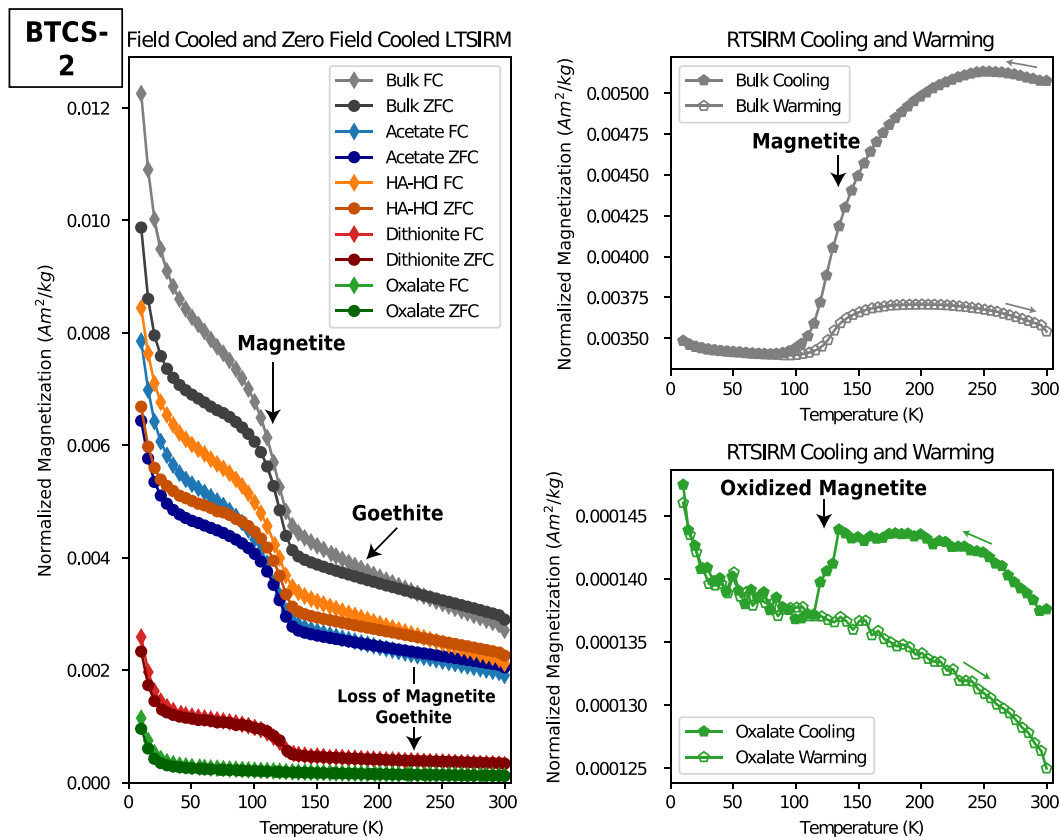
Figure 8. Magnetic analyses after each extraction for sample BTCS-2 (Holocene Baltic Sea, Baltic Ice Lake sediment) suggest that the sample contains magnetite, partially oxidized magnetite, and goethite based on its low-temperature behavior (annotated). During the acetate extraction, goethite and (oxidized) magnetite are slightly solubilized. Magnetite and/or partially oxidized magnetite is also slightly lost in the hydroxylamine-HCl (HA-HCl) extraction. Similarly to BTCS-1, the HA-HCl specimen has a slight stronger magnetization than the "previous" acetate specimen; we interpret that this is due to specimen differences from either the subsampling of initial powder, extraction protocol, and packing for magnetic analyses. During the dithionite extraction, goethite is effectively solubilized along with the majority of the (oxidized) magnetite as seen in both the low-temperature experiments and the coercivity spectra (Figure S15c). (Oxidized) magnetite continues to be solubilized during the oxalate extraction. See Figure 2 caption for abbreviations.

a large progressive decrease from 10 K all the way to 300 K during LTSIRM warming curves with higher remanence seen in FC LTSIRM experiments than ZFC LTSIRM experiments (Guyodo et al., 2003; Liu et al., 2006).

Goethite was identified in 14 of the 20 samples, and it dominated the LTSIRM warming curve behavior in five of these samples (GO130-286, MP-69.5, 15-TF-05-176, F849-225, and BS13-10A). The dithionite step was very effective in solubilizing goethite. The characteristic low-temperature magnetic behavior of goethite was gone following the dithionite extraction (e.g., SBC-1, GO130-286, and BTCS-2; Figures 2, 3, and 8) in all but one sample where some goethite remained (F849-225; Figure S8). This loss of magnetization is quantified and shown to be correlated to iron extracted by dithionite, especially for nanophase goethite (Figure S19). Notably, the four samples that had the largest quantity of iron dissolved during the dithionite step (>0.7 wt%) also contained abundant goethite (Figure S19). A high-coercivity phase observed in 10 samples is likely to be hematite. As mentioned earlier, hematite has a magnetic transition at ~250 K (the Morin transition), but it is often suppressed in naturally occurring hematite (Morin, 1950; J Wang et al., 2015) and was not conclusively identified in any of these samples. Although most of this high-coercivity phase was dissolved in the acetate step in some samples, we observed in three of the samples that the phase was removed during the dithionite step (e.g., MP-69.5, AMB4, and AMB6; Figure S3, S13c, and S7). These three samples did not all show large amounts of iron extracted during the dithionite extraction; as a result, we infer that iron from goethite typically dominates the operationally defined dithionite pool across sedimentary samples. Magnetic analyses suggest ferrihydrite/lepidocrocite (BTCS-1 and RI-07-07A-92; Figures 7 and S4) and maghemite (AMB4, AMB6, and BLKS-1; Figures 4, S13c, S7, and S12) are solubilized in the dithionite

extraction; when the hydroxylamine-HCl extraction was not applied, these minerals should probably be targeted by this extraction based on the operational definition of ferric iron oxides. Previous magnetic and spectroscopic analyses on synthetic, paleosol, and loess samples have shown that the dithionite extraction dissolves maghemite in addition to hematite (e.g., Fine & Singer, 1989; Singer et al., 1995; *W* Sun et al., 1995; van Oorschot, 2001; van Oorschot & Dekkers, 1999). Overall, of all the iron speciation extraction steps, the dithionite extraction is the most robust at extracting the targeted phases.

However, other phases were still dissolved during this extraction. Iron carbonates and iron sulfides that remained after the acetate extraction step continued to be dissolved in this step (siderite in SBC-1 and SGR-1; Figures 2 and S2 and iron sulfides in GP12-8B and BLKS-2, Figures 5, S12b, 6, and S15a). More striking is the dissolution of magnetite (and oxidized magnetite) during the dithionite extraction as noted in five samples. Magnetite was identified based on its characteristic Verwey transition at 120 K observed in RTSIRM and LTSIRM experiments (Verwey, 1939), and its presence was consistent with observed coercivity values (Peters & Dekkers, 2003). As magnetite oxidizes toward maghemite, the RTSIRM warming and cooling curves take on a hump-like form (Özdemir & Dunlop, 2010), which was used to qualitatively identify partially oxidized magnetite. Due to its strong magnetization, magnetite or oxidized magnetite were able to be identified in all 20 of the samples measured for this work. Of the five samples that showed a dissolution of magnetite in the dithionite step, ~25% to 75% of the magnetite was dissolved during the step (e.g., SBC-1 and BTCS-2; Figures 2, S13a, 8, and S15c), resulting in decreases in the coercivity spectra and decreased magnitude of the Verwey transition in low-temperature experiments. Previous magnetic analyses of synthetic, loess, and paleosol samples also show that magnetite is variably dissolved in dithionite extractions depending on its concentration and grain size (Hunt et al., 1995; van Oorschot, 2001; van Oorschot & Dekkers, 1999). In summary, the dithionite extraction will solubilize magnetite and continue to solubilize siderite and iron sulfides that were not previously removed.

3.4. Oxalate Extraction

The oxalate extraction was added in the most recent iron speciation protocol to target magnetite (Poulton & Canfield, 2005). Magnetite is the best characterized ferromagnetic mineral and can be uniquely identified particularly through identification of the low-temperature Verwey transition, which results in a decrease of remanent magnetization at ~120 K (Verwey, 1939). Magnetite, or partially oxidized magnetite, was identified in all 20 samples analyzed for this study. Some samples clearly show that the oxalate extraction solubilizes a portion of the magnetite (e.g., SBC-1 and SGR-1; Figures 2, S13a, and S2); in samples with the highest concentrations, ~25% to 75% of the remaining magnetite was dissolved (BTCS-1 and BTCS-2; Figures 7, 8, and S15). However, quantification of this magnetite is necessary to understand its importance for iron speciation. Saturation magnetization provides a method for quantification of magnetite when it is the only ferromagnetic mineral present; computing the difference in iron carried by magnetite between specimens after the dithionite extraction and after the oxalate extraction should equal the total amount of iron extracted by oxalate.

In most samples, after the dithionite extraction, magnetite was the dominant ferromagnetic mineral remaining. The three samples with magnetic iron sulfides were not included in this quantification and are discussed more below. Our magnetic quantification of magnetite highlights that the sedimentary rock samples contain <30 ppm of magnetite and the Baltic Sea Holocene sediments contain between 50 and 120 ppm of magnetite, although some magnetite was dissolved in earlier extractions before undergoing the oxalate step (Figure 9). In most cases, only a small portion of this magnetite is dissolved during the oxalate extraction, corroborating low-temperature data and coercivity spectra that show little or no change between these two steps (e.g., GO130-286, MP-69.5, 15-TF-05-176, and T095-53; Figures 3, S15b, S3, S4, and S10). Most strikingly, even if one assumed that all the magnetite was effectively solubilized by the oxalate extraction (using the value after the dithionite extraction before the oxalate extraction), the amount of iron extracted by the oxalate extraction is 1 to 3 orders of magnitude larger than the amount of iron carried by magnetite within the samples (Figure 9). Clearly, magnetite is not a large contributor to the pool of highly reactive iron in most samples and other mineral phases(s) are being solubilized during the oxalate step.

Low-temperature and coercivity spectra data allow for elimination of options of which other phases are solubilized by the oxalate step. Magnetic iron sulfides (greigite and monoclinic pyrrhotite) continue to be dissolved during this step (Figures 5, 6, S12b, and S15a); however, this dissolution can only account for some
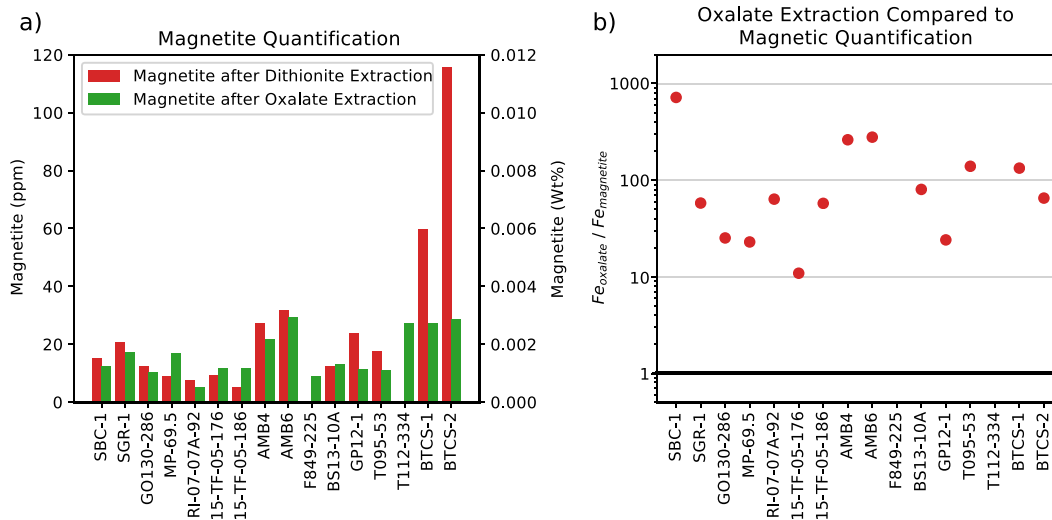
Figure 9. (a) Magnetite quantification based on saturation magnetization compared after the dithionite extraction (before the oxalate extraction) and after the oxalate extraction was applied. The amount of magnetite extracted during the oxalate extraction should be the difference between the two. Some samples show a gain in the amount of magnetite, which we attribute to the slight differences in the specimens (due to subsampling of the initial powder, extraction protocol, and packing for magnetic analyses) and/or the poorly constrained error bars of the saturation magnetization due to subtraction of a large paramagnetic component. (b) Comparison of the amount of iron solubilized during the oxalate extraction ($Fe_{oxalate}$) and the amount of iron carried by magnetite as quantified magnetically after the dithionite extraction ($Fe_{magnetite}$) plotted on a log scale. The thick black line emphasizes when the ratio is one, and iron amounts equal. Even if all the magnetite was extracted, $Fe_{oxalate}$ is 1 to 3 orders of magnitude higher than $Fe_{magnetite}$ suggesting that iron is being solubilized from another phase.

of the iron extracted in the oxalate step. The amount of iron extracted during the oxalate step in greigite-containing BLKS-1 and BLKS-2 is twice that extracted during the acetate step, even though the acetate step dissolved more greigite. One sample interpreted to contain siderite has additional loss of the mineral during the oxalate extraction (SBC-1; Figure 2). Two samples show a small loss in a high-coercivity component during the oxalate extraction, which is likely associated with dissolution of hematite (AMB4 and AMB6; Figures S13c and S7). While these three samples have large oxalate values, earlier losses in magnetization were much larger and comparison to the extracted iron pools suggests these minerals cannot account for all the iron extracted by oxalate. Overall, it appears that ferromagnetic minerals cannot explain the amount of iron being extracted during the oxalate step even though it is usually attributed to the mineral magnetite. While a decrease in high-field susceptibility is noted in all samples, this decrease is larger in samples with high-oxalate extractions (Figure S18), which suggests that a paramagnetic phase is being dissolved by the step.

Figure 10. X-ray diffraction quantification of clay minerals highlights a correlation between samples containing abundant chamosite and berthierine and those with a high quantity of iron solubilized during the oxalate extraction ($Fe_{oxalate}$). A linear regression of these clay abundances in the bulk specimens (as percent of total mineralogy) versus the $Fe_{oxalate}$ (weight percent) for the same sample is plotted ($R^2 = 0.40$, if only sedimentary rock samples are included $R^2 = 0.61$).

The high-angle clay-specific XRD analyses show a correlation between samples that have high-oxalate values and those containing berthierine and/or chamosite, suggesting these clay minerals are targeted during the oxalate extraction (Figure 10). Three sedimentary rock samples (SBC-1, AMB4, and AMB6) and two sediment samples (BTCS-1 and BTCS-2) have $Fe_{oxalate}$ values >0.5 wt%; these three sedimentary rock samples contain 2 to 8 times more berthierine and/or chamosite than other samples (except GP12-8B) (Figure 10 and Table S3). Berthierine ($(Fe,Al)_3(Si,Al)_2O_5(OH)_4$) is a Fe(II)-rich member of the serpentine subgroup most commonly associated with Phanerozoic shallow marine oolitic ironstones deposited in tropical environments, but it is also found in nonmarine settings including laterites and estuarine sediments. Some studies suggest berthierine accumulates via direct precipitation from the water column or
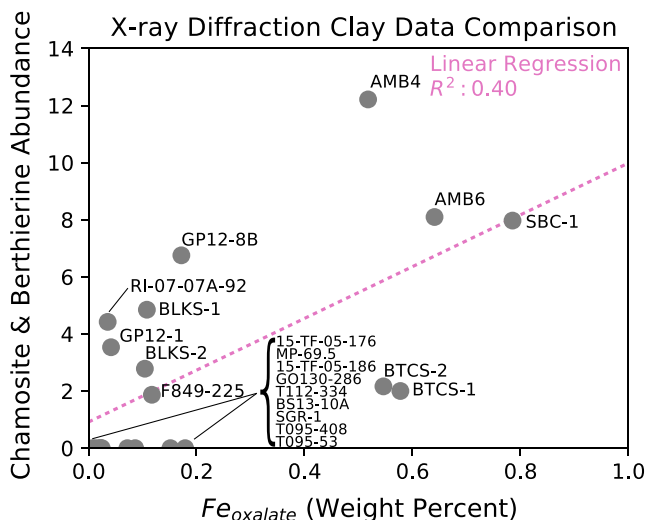
detrital transport, but it is predominantly thought to form during early diagenesis from precursors such as glauconite, kaolinite, odinite, or iron oxide (hydroxide) (Longstaffe, 2003; van Houten & Purucker, 1984). Chamosite $((Fe,Mg)_5Al(AlSi_3O_{10})(OH)_8)$ is a Fe(II)-rich chlorite that typically forms through the burial and diagenetic transformation of berthierine or kaolinite at temperatures ≥70 °C (Hornibrook & Longstaffe, 1996; Jahren & Aagaard, 1989; Velde et al., 1974). Due to chamosite and berthierine's structural similarity, their peaks at 7 and 3.55 Å lie close to each other and are difficult to distinguish using XRD. Assignment between the two phases was done based on whether a 14-Å peak was observed in the bulk scan and, if present, whether the peak intensity was significantly modulated compared to the 7-Å peak; if so, the clay is likely dominated by chamosite (although berthierine could also be present) and if not, vice versa. Although the clay analyses are precise, large error bars on the bulk analyses (up to 20%) make it difficult to place much weight on the quantification of individual specimens after each extraction. Even so, quantification of berthierine/chamosite highlights significant dissolution of these clays over the course of the protocol with a 10% to 80% decrease (except in BTCS-2) (Table S3). Five samples, SGR-1, SBC-1, GO130-286, BLKS-2, and BTCS-1, also showed significant loss of illite $(K,H_3O)(Al,Mg,Fe)_2(Si,Al)_4O_{10}[(OH)_2,(H2O)])$ (>50% decrease) occurring during the acetate, hydroxylamine-HCl, dithionite, or oxalate extractions (Table S3).

Both berthierine and chamosite (and illite) have variable chemical compositions with variable amounts of iron; the precise compositional range was not determined, and therefore, translation to weight percent and direct comparison with iron extracted by oxalate is not possible. The iron speciation sequential extraction protocol has also yet to be directly tested on these two minerals. However, there are indications in the literature that corroborate the idea that iron-bearing clays are the source of the iron extracted by oxalate. One study suggests that a museum-grade chamosite sample could be slightly dissolved in the dithionite extraction (Raiswell et al., 2011). Another study combining XRD and iron speciation showed that their samples all had high $Fe_{oxalate}$ (2.96 to 6.06 wt%) and also contained berthierine, chamosite, and glauconite (Tang et al., 2017). Overall, the oxalate extraction appears to solubilize iron-bearing silicates, specifically berthierine and/or chamosite.

4. Discussion

4.1. Comparison Between Targeted and Dissolved Mineralogy

The sequential extraction procedure developed by Poulton and Canfield (2005) has been widely used in paleoredox analyses, ancient and modern iron cycling studies, and other applications (e.g., Cai et al., 2018; Egger et al., 2016; Guilbaud et al., 2015; Poulton et al., 2010; Poulton & Canfield, 2011; Sperling et al., 2015; von der Heyden et al., 2018). Our results provide some support for connecting operationally defined iron pools to different mineralogical phases in complex natural samples and also highlight significant challenges in making such interpretations.

A major stated goal and result of the Poulton and Canfield (2005) sequential extraction procedure was the ability to isolate contributions of iron from Fe-bearing carbonate phases and from magnetite. In that work, the acetate extraction was argued to be effective at dissolving carbonate-associated iron while essentially leaving other phases unaffected. Our results show that the step is indeed effective at removing iron carried by carbonates and AVS, although depending on abundance/grain size/mineral-association, not all of these phases will be extracted. However, the step also leads to removal of ferromagnetic phases identified as iron oxides. These phases are difficult to quantify and often may only represent a small fraction of the extraction pool but in some cases could be a significant portion of the extraction pool and the highly reactive iron (>25%).

Our results show the dithionite extraction to be very effective in solubilizing goethite and most hematite within natural samples. Of all the extractions, it is the most effective at liberating the targeted minerals.

Poulton and Canfield (2005) found that the oxalate step was effective in solubilizing magnetite when it was the only phase and in a mixture of pure minerals. These results led to the conclusion that the step could be used to quantify the amount of magnetite in natural samples. Our findings contrast with this conclusion, revealing the extraction to be ineffective at fully solubilizing magnetite in natural rock and sediment samples. Furthermore, magnetite is typically present in amounts that are very low relative to the amount of

iron removed through the oxalate step. Rather, XRD analyses suggest that the oxalate step liberates iron from Fe-bearing clays, namely, berthierine and chamosite.

Given the complexity of phases that are actually targeted in each of the extractions, we recommend against using the mineral-specific names associated with each step. Our analyses demonstrate that most minerals were extracted, at least to a degree, across multiple different extractions. This is consistent with previous results by Poulton and Canfield (2005) demonstrating that some extractions were not perfectly specific (e.g., dithionite extracts some magnetite, Table 1 of that paper). While certain extractions dissolved the large majority of a mineral (e.g., dithionite for goethite), other phases such as monoclinic pyrrhotite, greigite, hematite, maghemite, and magnetite dissolved slowly throughout the sequential extraction procedure. Referring to the $Fe_{acetate}$ liberated iron as Fe_{carb} obscures that other phases are solubilized in this step, and referring to the $Fe_{oxalate}$ liberated iron as Fe_{mag} is largely incorrect. The solubility of minerals depends upon their grain size, crystallinity, and mineralogical association; our analyses of natural samples highlight the resulting variation and complexity of simple mineralogical assignments to chemical extraction pools. Distinct formation pathways and reaction rim formation both in sedimentary processes and during the extraction procedure are two mechanisms for these ranging solubilities. Future investigation in this regard could further elucidate iron cycling in both modern and ancient systems.

4.2. Implications for Paleoredox Interpretation

One perspective on these findings could be that the specific phases removed at each step are of little consequence given that almost all contribute to the highly reactive pool, which is typically compared en masse to pyrite and total iron for paleoredox interpretations. The iron speciation paleoredox proxy is operationally defined and empirically calibrated; therefore, the analyses here do not inherently invalidate it. However, there are multiple aspects of these results that raise questions related to paleoredox interpretations.

Although an empirically calibrated tool, iron speciation is theoretically grounded by the shelf-to-basin iron shuttle model (Lyons & Severmann, 2006). Iron is delivered into a basin in mineral phases containing ferric iron. In shallow waters (on the shelf), suboxic diagenesis will reduce the highly reactive phases, releasing ferrous iron. Although some iron is immediately reprecipitated and deposited, a small portion can be laterally transported to deeper in the basin as colloidal and particulate iron (oxyhydr)oxides (Lenstra et al., 2019). If anoxic waters are present in the deep basin, this highly reactive iron could accumulate and sediments will reflect this enrichment of highly reactive iron when compared to total iron. Similarly, euxinic waters will result in the majority of this highly reactive iron precipitating as pyrite due to the abundant sulfide. Geochemical iron speciation analyses on modern sediments provided foundations for this model in addition to guiding the calibration of the iron speciation paleoredox proxy (Raiswell & Canfield, 1998, 2012).

However, the initial empirical calibration for the highly reactive to total iron proxy ($Fe_{HR}/Fe_T > 0.38$) was only based on the dithionite extraction (and iron from CRS) (discussed in Farrell et al., 2013; Raiswell et al., 2018). The sequential procedure was developed later. Samples with high abundances of iron from the oxalate extraction could give ferruginous redox interpretations, potentially erroneously as our analyses highlight that iron-bearing clays are the main mineral being targeted in this extraction, not magnetite. The guiding principles behind the iron speciation proxy are that the solubilized minerals included in Fe_{HR} are highly reactive to sulfide on diagenetic time scales; it is unclear if this is true for these clay minerals, which predominantly form during early or burial diagenesis (with iron sourced from diverse possible precursors) and can also directly precipitate from the water column. Although ideally a new calibration of Fe_{HR}/Fe_T would be developed on modern sediments using the Poulton and Canfield (2005) extraction procedure (refining $Fe_{HR}/Fe_T > 0.38$), at the moment samples that contain high abundances of iron extracted in the oxalate pool should be flagged and more carefully investigated to understand their mineralogy and formation pathways.

Connecting iron speciation pools more directly to mineralogy also raises questions about the connection of this proxy to water column chemistry as opposed to postdepositional processes. For example, pyrrhotite, which we show to be removed in each extraction step (e.g., GP12-8B; Figure 5 and S12b), forms diagenetically, usually at the expense of other phases, primarily pyrite. Hot acid extractions performed on this sample did not reveal significant AVS, even though monoclinic pyrrhotite was readily detected magnetically. Previous literature has similarly noted poor extraction of pyrrhotite using the hot 6 N HCl method and

suggested the use of this methodology has led to widespread underestimation of monosulfides in ancient sedimentary rocks in the literature (Rice et al., 1993). Although the formation of pyrrhotite is thermodynamically limited at Earth surface temperatures (Horng & Roberts, 2006), experimental and geologic studies have shown that it can form at temperatures between 75 and 200 °C (Gillett, 2003; Hall, 1986; Kissin & Scott, 1982), a very low metamorphic grade that is quite common in ancient rocks targeted for paleoredox investigations. As a result, pyrrhotite's presence in rocks can greatly affect the pyrite to highly reactive iron proxy (Fe_{py}/Fe_{HR}) leading to interpretations that do not reflect water column chemistry (Slotznick, Eiler, et al., 2018). Some studies that identified pyrrhotite in their samples attempted to correct for its presence (e.g., Reuschel et al., 2012); our analyses highlight the difficulty of doing so since a single extraction does not represent all the pyrrhotite.

Although we have noted that the dithionite extraction is one of the most robust extractions, our data reveal an abundance of goethite throughout the sedimentary rock samples (Figure S19), which accordingly has a significant influence on the highly reactive iron values. Although goethite has been shown to form during early sedimentary diagenesis (van der Zee et al., 2003), it is also a common product of surficial oxidative weathering and often assumed to be a modern weathering overprint. At the surface, goethite can form at the expense of other iron oxides and iron sulfides (Bedarida & Pedemonte, 1971; Bladh, 1982), but also can form from Fe-silicate minerals and precipitate from groundwater (liesegang banding) (Eggleton et al., 1987; Gilkes & Suddhiprakarn, 1979; Ortoleva et al., 1986; Schwertmann, 1988). Paleomagnetic studies on sedimentary rocks reveal that goethite often records the present local magnetic field (indicating recent formation) and comparison between surface outcrop samples and deep drill cores corroborates its formation during recent near-surface processes (e.g., Belkaaloul & Aïssaoui, 1997; Sprain et al., 2018; Swanson-Hysell et al., 2012). The prevalence of goethite in the analyzed sample suite raises questions about mineralogical transformations that occurred during surface weathering or powder storage. Better understanding of the primary nature of goethite and its formation pathways is important for interpreting the dithionite extraction pool. Rock magnetic screening of samples for the presence of goethite could be a valuable addition to iron speciation studies.

Hematite, maghemite, and partially oxidized magnetite are noted throughout our sample suite; they are solubilized throughout the acetate, hydroxylamine-HCl, and dithionite extractions. These phases often coexist in our samples (along with goethite and/or ferrihydrite) and are the result of oxidative reaction pathways; however, it is unclear when these reactions occurred. This mineral mixture could be inherited from the protolith, form during weathering and fluvial transport, or relate to water column and pore water redox cycling during deposition and early diagenesis. During this portion of the sedimentary cycle, these highly reactive phases represent oxidizing conditions but contribute to the highly reactive iron pool, which without additional context could be interpreted as representing deposition beneath a ferruginous water column. Although potentially not an issue in off-shore basins, analysis of lacustrine shallow-water red siltstones shows that the presence of hematite can lead to erroneous paleoredox interpretations (Slotznick, Swanson-Hysell, et al., 2018). Additionally, this suite of iron oxides could form in significantly later postdepositional processes associated with diagenesis/low-grade metamorphism or more recent surficial weathering. Postdepositional formation of hematite can be at the expense of other highly reactive phases like pyrite, (oxy)hydroxides, magnetite, and carbonates (e.g., Anand & Gilkes, 1984; Elmore et al., 1985; Jiang et al., 2015; Weil & Van der Voo, 2002) and can also occur due to reactions of iron-bearing clays and silicates (Lu et al., 1994; Turner, 1979; Walker et al., 1981). Such a movement of iron from the unreactive iron pool to the highly reactive pool through oxic reactions could incorrectly suggest depositional conditions were ferruginous. Although mineral-specific techniques are sometimes more qualitative or time-consuming, focusing on mineralogy is vital in studies of iron biogeochemical cycling as these processes are fundamentally dependent on mineral reactions.

Quantification of magnetite in weight percent in sediments using nongeochemical techniques has not been the norm in the past two decades although exceptions exist (e.g., Huberty et al., 2012; Hurowitz et al., 2017; Slotznick et al., 2019; Slotznick, Swanson-Hysell, et al., 2018). Previous work on subgreenschist fine-grained siliciclastics similarly noted magnetite levels at <30 ppm in two sample suites similar to this work (Slotznick et al., 2019; van Oorschot et al., 2001) but up to 570-ppm magnetite in another site (Slotznick, Swanson-Hysell, et al., 2018). These results suggest that provenance, water column reactions, and diagenesis all
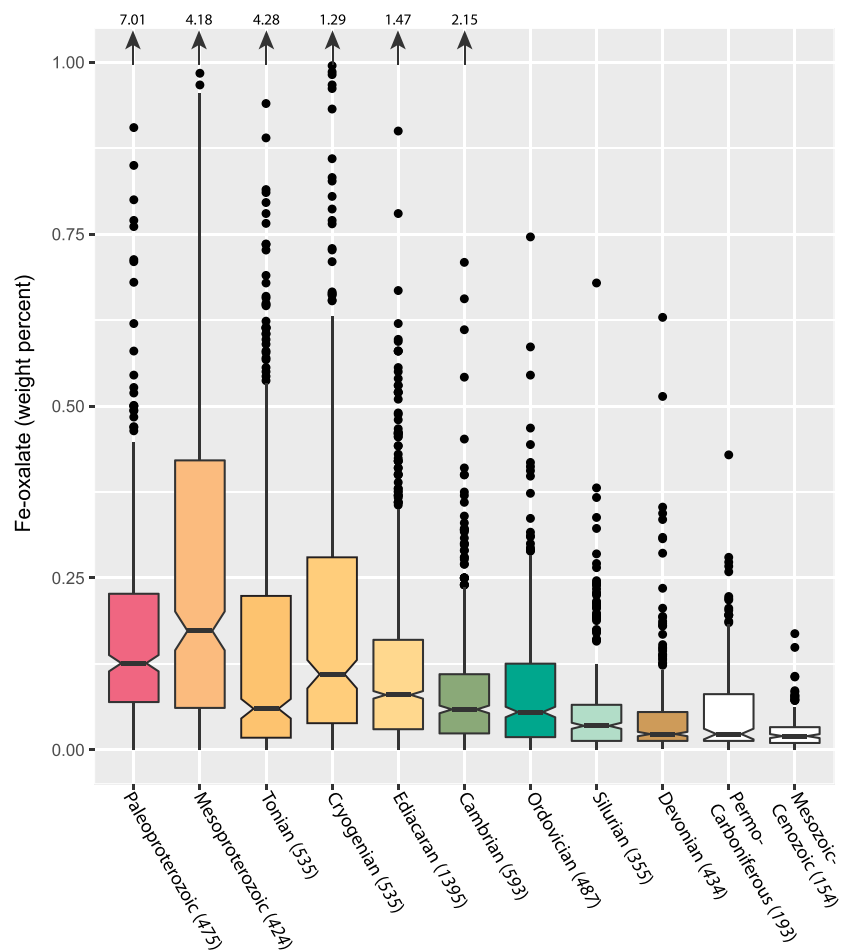
Figure 11. Box and whiskers plot of weight percent iron solubilized by the oxalate extraction in a collection of samples binned by era or period across geologic time. All values are associated with the final step of the sequential extraction protocol following Poulton and Canfield [2005; e.g., the oxalate extraction following the acetate and dithionite extractions] (Table S4). The y axis stops at 1.0 wt% to better visualize changes in the median and interquartile range. Arrows at the top of the plot point to the maximum value in each time bin; post-Cambrian time bins do not have maximum Fe-oxalate values >0.75 wt%. Sample numbers in each bin are shown next to the bin name, and era/period ages are as follows: Paleoproterozoic 2500–1600 Ma, Mesoproterozoic 1600–1000 Ma, Tonian 1000–720 Ma, Cryogenian 720–635 Ma, Ediacaran 635–541 Ma, Cambrian 541–485 Ma, Ordovician 485–444 Ma, Silurian 444–419 Ma, Devonian 419–359 Ma, Permo-Carboniferous 359–252 Ma, and Mesozoic-Cenozoic 252–0 Ma.

play important roles in magnetite preservation and sedimentary iron cycling. While the typical quantity of magnetite in sediments can make detection difficult through chemical extraction, synchrotron X-ray spectroscopy and magnetic techniques, both sensitive to mineralogy at the parts per billion level, can be key tools for work on magnetite's role in iron cycling moving forward.

The observation that the oxalate extraction is not removing magnetite, but rather other iron-bearing minerals (suggested here to be berthierine and/or chamosite), begs the question of how this affects our interpretation of the geochemical record through Earth History. A preliminary investigation of the Fe$_{oxalate}$ pool through geologic time is presented here. We analyzed 5,388 samples through geologic time; this was based on the compilation of Sperling et al. (2015) with 2,124 published and new Fe$_{oxalate}$ measurements (all generated at Stanford following protocols described in the section 2.2) included to increase Phanerozoic data coverage (note though that post-Paleozoic sampling remains scarce). This analysis shows an intriguing trend in iron extracted by oxalate (Figure 11), with median values of 0.14 and 0.18 wt% for the Paleoproterozoic and Mesoproterozoic bins, intermediate values for the Neoproterozoic and Cambro-Ordovician bins (0.11 to 0.055 wt%) and lower values for younger time periods (0.035 to 0.02 wt%). Maximum values will be strongly controlled by sampling effects, but there is a large decrease in maximum values through time

within the current data set as well as the 75th percentile (Figure 11). Nonparametric Steel-Dwass tests indicate that the Paleoproterozoic and Mesoproterozoic are not statistically different from each other ($p = 0.87$), but with occasional exceptions both are statistically higher than all younger bins (generally $p < 0.001$). Further, Neoproterozoic bins are almost always significantly higher than Phanerozoic bins (again, generally $p < 0.001$). Decision-tree analysis suggests that the major change in terms of $Fe_{oxalate}$ contents is between Cryogenian and older samples and Ediacaran and younger samples. More samples and statistical analyses controlling for spatial-temporal sampling density will provide added insight, but at a first order, this trend of higher $Fe_{oxalate}$ in older samples will likely remain robust.

On a pragmatic level, these results indicate that the misclassification of the mineralogy of iron pools as indicated by our magnetic experiments will dominantly affect redox interpretations of Proterozoic iron speciation data as compared to Phanerozoic data. Additionally, the use of empirical calibrations from modern sediments to interpret ancient rocks is challenged as the $Fe_{oxalate}$ pool does not appear to be present in appreciable quantities in the modern and geologically recent systems.

These results also point to significant changes in the history of iron cycling, although exactly what this represents must remain fairly speculative as at present our data only reveal a positive correlation between $Fe_{oxalate}$ and berthierine/chamosite abundance within the samples. Recent papers have suggested higher levels of authigenic clay formation during the Proterozoic than in the Phanerozoic based on occurrence data, carbon cycle modeling, and silicon isotopes (Isson & Planavsky, 2018; Trower & Fischer, 2019). If $Fe_{oxalate}$ can be definitively linked to berthierine/chamosite, the oxalate-extractable iron record through time (Figure 11) would provide support for the hypothesized decrease in authigenic clay formation near the end of the Neoproterozoic. These results emphasize the importance of studying mineralogical changes as a window into global biogeochemical cycling.

5. Conclusions

We present one of the first tests of the standardized sequential extraction for iron speciation using natural samples. These results highlight the subtlety and complexity of dealing with natural samples that contain diverse mineral assemblages. The magnetic and XRD measurements made on specimens stopped after each extraction step provide an independent method for identifying and quantifying what iron-bearing minerals were dissolved. The dithionite extraction stands out as the most robust at effectively solubilizing the targeted mineralogy of ferric iron oxides. The oxalate extraction appears to primarily dissolve iron-bearing clays, specifically berthierine/chamosite, not the targeted mineral magnetite which is present only in low abundances. The analyses also emphasize that the solubility of minerals depends upon various factors (such as grain size, crystallinity, and association) resulting in natural variation and complexity, which must be taken into account when utilizing sequential extraction methods. Studies of past and present iron cycling should choose multipronged methodologies to provide more direct connections to mineralogy and thus natural processes.

References

Aharoni, A., Frei, E., & Schieber, M. (1962). Some properties of γ-Fe2O3 obtained by hydrogen reduction of α-Fe2O3. *JPCS*, *23*(6), 545–554. https://doi.org/10.1016/0022-3697(62)90512-7

Anand, R., & Gilkes, R. (1984). Mineralogical and chemical properties of weathered magnetite grains from lateritic saprolite. *J. Soil Sci.*, *35*(4), 559–567. https://doi.org/10.1111/j.1365-2389.1984.tb00613.x

APHA (2005). *Standard methods for the examination of water and wastewater*. Washington, DC, USA: American Public Health Association (APHA).

Bacon, J. R., & Davidson, C. M. (2008). Is there a future for sequential chemical extraction? *Analyst*, *133*(1), 25–46. https://doi.org/10.1039/b711896a

Bate, G. (1980). Recording materials. In E. P. Wohlfarth (Ed.), *Handbook of ferromagnetic materials* (Vol. 2, pp. 381–507). North Holland: Elsevier Science, B.V. https://doi.org/10.1016/S1574-9304(05)80108-7

Bedarida, F., & Pedemonte, G. (1971). Hematite to goethite surface weathering. *American Mineralogist*, *56*(7-8), 1469–1473.

Belkaaloul, N. K., & Aïssaoui, D. M. (1997). Nature and origin of magnetic minerals within the Middle Jurassic shallow-water carbonate rocks of the Paris Basin, France: Implications for magnetostratigraphic dating. *Geophysical Journal International*, *130*(2), 411–421. https://doi.org/10.1111/j.1365-246x.1997.tb05657.x

Berner, R. A. (1970). Sedimentary pyrite formation. *Am. J. Sci.*, *268*(1), 1–23. https://doi.org/10.2475/ajs.268.1.1

Berquó, T. S., Banerjee, S. K., Ford, R. G., Penn, R. L., & Pichler, T. (2007). High crystallinity Si-ferrihydrite: An insight into its Néel temperature and size dependence of magnetic properties. *JGRB*, *112*(B2). https://doi.org/10.1029/2006jb004583

Besnus, M., & Meyer, A. (1964). Nouvelles données expérimentales sur le magnétisme de la pyrrhotine naturelle. *Proc. Int. Conf. Mag., Nottingham*, 507–511.

Bladh, K. W. (1982). The formation of goethite, jarosite, and alunite during the weathering of sulfide-bearing felsic rocks. *Econ. Geol.*, 77(1), 176–184. https://doi.org/10.2113/gsecongeo.77.1.176

Burton, E. D., Sullivan, L. A., Bush, R. T., Johnston, S. G., & Keene, A. F. (2008). A simple and inexpensive chromium-reducible sulfur method for acid-sulfate soils. *Appl. Geochem.*, 23(9), 2759–2766. https://doi.org/10.1016/j.apgeochem.2008.07.007

Cai, C., Leu, A. O., Xie, G.-J., Guo, J., Feng, Y., Zhao, J.-X., et al. (2018). A methanotrophic archaeon couples anaerobic oxidation of methane to Fe (III) reduction. *The ISME journal*, 1. https://doi.org/10.1038/s41396-018-0109-x

Canfield, D. E., Raiswell, R., Westrich, J. T., Reaves, C. M., & Berner, R. A. (1986). The use of chromium reduction in the analysis of reduced inorganic sulfur in sediments and shales. *Chem. Geol.*, 54(1), 149–155. https://doi.org/10.1016/0009-2541(86)90078-1

Claff, S. R., Sullivan, L. A., Burton, E. D., & Bush, R. T. (2010). A sequential extraction procedure for acid sulfate soils: Partitioning of iron. *Geoderma*, 155(3-4), 224–230. https://doi.org/10.1016/j.geoderma.2009.12.002

Clark, D. (1984). Hysteresis properties of sized dispersed monoclinic pyrrhotite grains. *Geophysical Research Letters*, 11(3), 173–176. https://doi.org/10.1029/gl011i003p00173

Cornwell, J. C., & Morse, J. W. (1987). The characterization of iron sulfide minerals in anoxic marine sediments. *Mar. Chem.*, 22(2), 193–206. https://doi.org/10.1016/0304-4203(87)90008-9

Dekkers, M. (1988). Magnetic properties of natural pyrrhotite Part I: Behaviour of initial susceptibility and saturation-magnetization-related rock-magnetic parameters in a grain-size dependent framework. *Physics of the Earth and Planetary Interiors*, 52(3-4), 376–393. https://doi.org/10.1016/0031-9201(88)90129-x

Dekkers, M. (1989a). Magnetic properties of natural goethite—II. TRM behaviour during thermal and alternating field demagnetization and low-temperature treatment. *Geophysical Journal International*, 97(2), 341–355. https://doi.org/10.1111/j.1365-246x.1989.tb00505.x

Dekkers, M. (1989b). Magnetic properties of natural goethite—I. Grain-size dependence of some low-and high-field related rockmagnetic parameters measured at room temperature. *Geophysical Journal International*, 97(2), 323–340. https://doi.org/10.1111/j.1365-246x.1989.tb00504.x

Dijkstra, N., Slomp, C. P., & Behrends, T. (2016). Vivianite is a key sink for phosphorus in sediments of the Landsort Deep, an intermittently anoxic deep basin in the Baltic Sea. *Chem. Geol.*, 438, 58–72. https://doi.org/10.1016/j.chemgeo.2016.05.025

Dunlop, D. J. (1986). Hysteresis properties of magnetite and their dependence on particle size: A test of pseudo-single-domain remanence models. *JGRB*, 91(B9), 9569–9584. https://doi.org/10.1029/jb091ib09p09569

Egger, M., Kraal, P., Jilbert, T., Sulu-Gambari, F., Sapart, C. J., Röckmann, T., & Slomp, C. P. (2016). Anaerobic oxidation of methane alters sediment records of sulfur, iron and phosphorus in the Black Sea. *BGeo*, 13(18), 5333. https://doi.org/10.5194/bg-13-5333-2016

Egger, M., Rasigraf, O., Sapart, C. L. J., Jilbert, T., Jetten, M. S., Röckmann, T., et al. (2015). Iron-mediated anaerobic oxidation of methane in brackish coastal sediments. *Environ. Sci. Technol.*, 49(1), 277–283. https://doi.org/10.1021/es503663z

Eggleton, R. A., Foudoulis, C., & Varkevisser, D. (1987). Weathering of basalt: Changes in rock chemistry and mineralogy. *Clays Clay Miner.*, 35(3), 161–169. https://doi.org/10.1346/ccmn.1987.0350301

Elmore, R. D., Dunn, W., & Peck, C. (1985). Absolute dating of dedolomitization by means of paleomagnetic techniques. *Geology*, 13(8), 558–561. https://doi.org/10.1130/0091-7613(1985)13<558:adodbm>2.0.co;2

Farrell, Ú. C., Briggs, D. E., Hammarlund, E. U., Sperling, E. A., & Gaines, R. R. (2013). Paleoredox and pyritization of soft-bodied fossils in the Ordovician Frankfort Shale of New York. *Am. J. Sci.*, 313(5), 452–489. https://doi.org/10.2475/05.2013.02

Fine, P., & Singer, M. (1989). Contribution of ferrimagnetic minerals to oxalate-and dithionite-extractable iron. *Soil Science Society of America Journal*, 53(1), 191–196. https://doi.org/10.2136/sssaj1989.03615995005300010035x

Frederichs, T., Von Dobeneck, T., Bleil, U., & Dekkers, M. (2003). Towards the identification of siderite, rhodochrosite, and vivianite in sediments by their low-temperature magnetic properties. *Physics and Chemistry of the Earth. Parts A/B/C*, 28(16-19), 669–679. https://doi.org/10.1016/s1474-7065(03)00121-9

Garrick-Bethell, I., Weiss, B. P., Shuster, D. L., & Buz, J. (2009). Early lunar magnetism. *Sci*, 323(5912), 356–359. https://doi.org/10.1126/science.1166804

Gilkes, R., & Suddhiprakarn, A. (1979). Biotite alteration in deeply weathered granite. I. Morphological, mineralogical, and chemical properties. *Clays Clay Miner.*, 27(5), 349–360. https://doi.org/10.1346/ccmn.1979.0270505

Gillett, S. L. (2003). Paleomagnetism of the Notch Peak contact metamorphic aureole, revisited: Pyrrhotite from magnetite+ pyrite under submetamorphic conditions. *JGRB*, 108(B9). https://doi.org/10.1029/2002jb002386

Guilbaud, R., Poulton, S. W., Butterfield, N. J., Zhu, M., & Shields-Zhou, G. A. (2015). A global transition to ferruginous conditions in the early Neoproterozoic oceans. *Nature Geoscience*, 8(6), 466. https://doi.org/10.1038/ngeo2434

Guyodo, Y., Banerjee, S. K., Penn, R. L., Burleson, D., Berquo, T. S., Seda, T., & Solheid, P. (2006). Magnetic properties of synthetic six-line ferrihydrite nanoparticles. *Physics of the Earth and Planetary Interiors*, 154(3-4), 222–233. https://doi.org/10.1016/j.pepi.2005.05.009

Guyodo, Y., Bonville, P., Till, J. L., Ona-Nguema, G., Lagroix, F., & Menguy, N. (2016). Constraining the origins of the magnetism of lepidocrocite (γ-FeOOH): A Mössbauer and magnetization study. *Frontiers in Earth Science*, 4, 28. https://doi.org/10.3389/feart.2016.00028

Guyodo, Y., Mostrom, A., Lee Penn, R., & Banerjee, S. K. (2003). From nanodots to nanorods: Oriented aggregation and magnetic evolution of nanocrystalline goethite. *Geophysical Research Letters*, 30(10). https://doi.org/10.1029/2003gl017021

Hall, A. J. (1986). Pyrite-pyrrhotine redox reactions in nature. *Mineralogical Magazine*, 50, 223–229. https://doi.org/10.1180/minmag.1986.050.356.05

Heider, F., Zitzelsberger, A., & Fabian, K. (1996). Magnetic susceptibility and remanent coercive force in grown magnetite crystals from 0.1 μm to 6 mm. *PEPI*, 93(3-4), 239–256. https://doi.org/10.1016/0031-9201(95)03071-9

Hirt, A., Lanci, L., Dobson, J., Weidler, P., & Gehring, A. (2002). Low-temperature magnetic properties of lepidocrocite. *Journal of Geophysical Research: Solid Earth*, 107(B1), EPM 5-1–EPM 5-9. https://doi.org/10.1029/2001jb000242

Horng, C. S., & Roberts, A. P. (2006). Authigenic or detrital origin of pyrrhotite in sediments?: Resolving a paleomagnetic conundrum. *Earth and Planetary Science Letters*, 241(3), 750–762. https://doi.org/10.1016/j.epsl.2005.11.008

Horng, C. S., & Roberts, A. P. (2018). The low-temperature Besnus magnetic transition: Signals due to monoclinic and hexagonal pyrrhotite. *Geochem. Geophys. Geosyst.*, 19(9), 3364–3375. https://doi.org/10.1029/2017gc007394

Hornibrook, E. R., & Longstaffe, F. J. (1996). Berthierine from the lower cretaceous Clearwater formation, Alberta, Canada. *Clays Clay Miner.*, 44(1), 1–21. https://doi.org/10.1346/ccmn.1996.0440101

Housen, B. A., Banerjee, S., & Moskowitz, B. (1996). Low-temperature magnetic properties of siderite and magnetite in marine sediments. *Geophysical Research Letters*, *23*(20), 2843–2846. https://doi.org/10.1029/96gl01197

Hu, S., Appel, E., Hoffmann, V., Schmahl, W. W., & Wang, S. (1998). Gyromagnetic remanence acquired by greigite (Fe3S4) during static three-axis alternating field demagnetization. *Geophysical Journal International*, *134*(3), 831–842. https://doi.org/10.1046/j.1365-246x.1998.00627.x

Hu, S., Stephenson, A., & Appel, E. (2002). A study of gyroremanent magnetisation (GRM) and rotational remanent magnetisation (RRM) carried by greigite from lake sediments. *Geophysical Journal International*, *151*(2), 469–474. https://doi.org/10.1046/j.1365-246x.2002.01793.x

Huberty, J. M., H. Konishi, P. R. Heck, J. H. Fournelle, J. W. Valley, & H. Xu (2012). Silician magnetite from the Dales Gorge member of the Brockman iron formation, Hamersley Group, Western Australia. *American Minerologist*, *97*(1), 26–37. https://doi.org/10.2138/am.2012.3864

Hunt, C. P., Singer, M. J., Kletetschka, G., TenPas, J., & Verosub, K. L. (1995). Effect of citrate-bicarbonate-dithionite treatment on fine-grained magnetite and maghemite. *Earth and Planetary Science Letters*, *130*(1-4), 87–94. https://doi.org/10.1016/0012-821x(94)00256-x

Hurowitz, J. A., Grotzinger, J. P., Fischer, W. W., McLennan, S. M., Milliken, R. E., Stein, N., et al. (2017). Redox stratification of an ancient lake in Gale crater, Mars. *Science*, *356*(6341), eaah6849. https://doi.org/10.1126/science.aah6849

Isson, T. T., & Planavsky, N. J. (2018). Reverse weathering as a long-term stabilizer of marine pH and planetary climate. *Nature*, *560*(7719), 471. https://doi.org/10.1038/s41586-018-0408-4

Jahren, J., & Aagaard, P. (1989). Compositional variations in diagenetic chlorites and illites, and relationships with formation-water chemistry. *Clay Minerals*, *24*(2), 157–170. https://doi.org/10.1180/claymin.1989.024.2.04

Jiang, Z., Liu, Q., Dekkers, M. J., Tauxe, L., Qin, H., Barrón, V., & Torrent, J. (2015). Acquisition of chemical remanent magnetization during experimental ferrihydrite-like–hematite conversion in Earth-like magnetic field—implications for paleomagnetic studies of red beds. *Earth and Planetary Science Letters*, *428*, 1–10. https://doi.org/10.1016/j.epsl.2015.07.024

Johnston, D., Poulton, S., Tosca, N., O'brien, T., Halverson, G., Schrag, D., & Macdonald, F. (2013). Searching for an oxygenation event in the fossiliferous Ediacaran of northwestern Canada. *Chem. Geol.*, *362*, 273–286. https://doi.org/10.1016/j.chemgeo.2013.08.046

Kars, M., Lerouge, C., Grangeon, S., Aubourg, C., Tournassat, C., Madé, B., & Claret, F. (2015). Identification of nanocrystalline goethite in reduced clay formations: Application to the Callovian-Oxfordian formation of Bure (France). *American Mineralogist*, *100*(7), 1544–1553. https://doi.org/10.2138/am-2015-5096

Kirschvink, J. L., Kopp, R. E., Raub, T. D., Baumgartner, C. T., & Holt, J. W. (2008). Rapid, precise, and high-sensitivity acquisition of paleomagnetic and rock-magnetic data: Development of a low-noise automatic sample changing system for superconducting rock magnetometers. *Geochemistry Geophysics Geosystems*, *9*(5), Q05Y01. https://doi.org/10.1029/2007gc001856

Kissin, S., & Scott, S. (1982). Phase relations involving pyrrhotite below 350 °C. *Econ. Geol.*, *77*(7), 1739–1754. https://doi.org/10.2113/gsecongeo.77.7.1739

Klein, F., Bach, W., Humphris, S. E., Kahl, W.-A., Jöns, N., Moskowitz, B., & Berquó, T. S. (2014). Magnetite in seafloor serpentinite—Some like it hot. *Geology*, *42*(2), 135–138. https://doi.org/10.1130/g35068.1

Kunzmann, M., Halverson, G. P., Scott, C., Minarik, W. G., & Wing, B. A. (2015). Geochemistry of Neoproterozoic black shales from Svalbard: Implications for oceanic redox conditions spanning Cryogenian glaciations. *Chem. Geol.*, *417*, 383–393. https://doi.org/10.1016/j.chemgeo.2015.10.022

La Force, M. J., & Fendorf, S. (2000). Solid-phase iron characterization during common selective sequential extractions. *Soil Science Society of America Journal*, *64*(5), 1608–1615. https://doi.org/10.2136/sssaj2000.6451608x

Lenstra, W., Hermans, M., Séguret, M., Witbaard, R., Behrends, T., Dijkstra, N., et al. (2019). The shelf-to-basin iron shuttle in the Black Sea revisited. *Chem. Geol.*, *511*, 314–341. https://doi.org/10.1016/j.chemgeo.2018.10.024

Liu, Q., Yu, Y., Torrent, J., Roberts, A. P., Pan, Y., & Zhu, R. (2006). Characteristic low-temperature magnetic properties of aluminous goethite [α-(Fe, Al) OOH] explained. *Journal of Geophysical Research: Solid Earth*, *111*(B12). https://doi.org/10.1029/2006jb004560

Longstaffe, F. J. (2003). Berthierine. In G. V. Middleton, M. J. Church, M. Coniglio, L. A. Hardie, F. J. Longstaffe (Eds.) *Sedimentology* (pp. 104–108). Dordrecht: Springer Netherlands. https://doi.org/10.1007/978-1-4020-3609-5_26

Lu, G., McCabe, C., Henry, D. J., & Schedl, A. (1994). Origin of hematite carrying a Late Paleozoic remagnetization in a quartz sandstone bed from the Silurian Rose Hill Formation, Virginia, USA. *Earth and Planetary Science Letters*, *126*(4), 235–246. https://doi.org/10.1016/0012-821x(94)90109-0

Lyons, T. W., & Severmann, S. (2006). A critical look at iron paleoredox proxies: New insights from modern euxinic marine basins. *Geochim. Cosmochim. Acta*, *70*(23), 5698–5722. https://doi.org/10.1016/j.gca.2006.08.021

Michel, F. M., Barrón, V., Torrent, J., Morales, M. P., Serna, C. J., Boily, J.-F., et al. (2010). Ordered ferrimagnetic form of ferrihydrite reveals links among structure, composition, and magnetism. *PNAS*, *107*(7), 2787–2792. https://doi.org/10.1073/pnas.0910170107

Morin, F. (1950). Magnetic susceptibility of αFe_2O_3 and αFe_2O_3 with added titanium. *Physical Review*, *78*(6), 819. https://doi.org/10.1103/physrev.78.819.2

Ortoleva, P., Auchmuty, G., Chadam, J., Hettmer, J., Merino, E., Moore, C., & Ripley, E. (1986). Redox front propagation and banding modalities. *Physica D: Nonlinear Phenomena*, *19*(3), 334–354. https://doi.org/10.1016/0167-2789(86)90063-1

Özdemir, Ö., & Dunlop, D. J. (2010). Hallmarks of maghemitization in low-temperature remanence cycling of partially oxidized magnetite nanoparticles. *Journal of Geophysical Research*, *115*, B02101. https://doi.org/10.1029/2009jb006756

Özdemir, Ö., & Dunlop, D. J. (2014). Hysteresis and coercivity of hematite. *Journal of Geophysical Research: Solid Earth*, *119*(4), 2582–2594. https://doi.org/10.1002/2013JB010739

Pauthenet, R. (1950). Variation thermique de l'aimantation spontanée des ferrites de nickel, cobalt, fer et manganèse. *Comptes Rendus de l'Académie des Sciences*, *230*(21), 1842–1843.

Peters, C., & Dekkers, M. (2003). Selected room temperature magnetic parameters as a function of mineralogy, concentration and grain size. *Physics and Chemistry of the Earth*, *28*(16), 659–667. https://doi.org/10.1016/s1474-7065(03)00120-7

Poulton, S. W., & Canfield, D. E. (2005). Development of a sequential extraction procedure for iron: Implications for iron partitioning in continentally derived particulates. *Chem. Geol.*, *214*(3), 209–221. https://doi.org/10.1016/j.chemgeo.2004.09.003

Poulton, S. W., & Canfield, D. E. (2011). Ferruginous conditions: A dominant feature of the ocean through Earth's history. *Elements*, *7*(2), 107–112. https://doi.org/10.2113/gselements.7.2.107

Poulton, S. W., P. W. Fralick, and D. E. Canfield (2004), The transition to a sulphidic ocean ~1.84 billion years ago, *Nature*, *431*(7005), 173-177. https://doi.org/10.1038/nature02912

Poulton, S. W., Fralick, P. W., & Canfield, D. E. (2010). Spatial variability in oceanic redox structure 1.8 billion years ago. *Nature Geoscience*, *3*(7), 486–490. https://doi.org/10.1038/ngeo889

Praharaj, T., & Fortin, D. (2004). Determination of acid volatile sulfides and chromium reducible sulfides in Cu-Zn and Au mine tailings, Water, Air. *Soil Pollut.*, *155*(1-4), 35–50. https://doi.org/10.1023/b:wate.0000026526.26339.c3

Raiswell, R., Canfield, D., & Berner, R. (1994). A comparison of iron extraction methods for the determination of degree of pyritisation and the recognition of iron-limited pyrite formation. *Chem. Geol.*, *111*(1), 101–110. https://doi.org/10.1016/0009-2541(94)90084-1

Raiswell, R., & Canfield, D. E. (1998). Sources of iron for pyrite formation in marine sediments. *Am. J. Sci.*, *298*(3), 219–245. https://doi.org/10.2475/ajs.298.3.219

Raiswell, R., & Canfield, D. E. (2012). The iron biogeochemical cycle past and present. *Geochemical Perspectives*, *1*(1), 1–2. https://doi.org/10.7185/geochempersp.1.1

Raiswell, R., Hardisty, D. S., Lyons, T. W., Canfield, D. E., Owens, J. D., Planavsky, N. J., et al. (2018). The iron paleoredox proxies: A guide to the pitfalls, problems and proper practice. *Am. J. Sci.*, *318*(5), 491–526. https://doi.org/10.2475/05.2018.03

Raiswell, R., Reinhard, C. T., Derkowski, A., Owens, J., Bottrell, S. H., Anbar, A. D., & Lyons, T. W. (2011). Formation of syngenetic and early diagenetic iron minerals in the late Archean Mt. McRae Shale, Hamersley Basin, Australia: New insights on the patterns, controls and paleoenvironmental implications of authigenic mineral formation. *Geochim. Cosmochim. Acta*, *75*(4), 1072–1087. https://doi.org/10.1016/j.gca.2010.11.013

Reinhard, C. T., Raiswell, R., Scott, C., Anbar, A. D., & Lyons, T. W. (2009). A late Archean sulfidic sea stimulated by early oxidative weathering of the continents. *Sci*, *326*(5953), 713–716. https://doi.org/10.1126/science.1176711

Reuschel, M., Melezhik, V., & Strauss, H. (2012). Sulfur isotopic trends and iron speciation from the c. 2.0 Ga Pilgujärvi Sedimentary Formation, NW Russia. *Precambrian Res*, *196*, 193–203. https://doi.org/10.1016/j.precamres.2011.12.009

Rice, C. A., Tuttle, M. L., & Reynolds, R. L. (1993). The analysis of forms of sulfur in ancient sediments and sedimentary rocks: Comments and cautions. *Chem. Geol.*, *107*(1-2), 83–95. https://doi.org/10.1016/0009-2541(93)90103-p

Richter, C., & van der Pluijm, B. A. (1994). Separation of paramagnetic and ferrimagnetic susceptibilities using low temperature magnetic susceptibilities and comparison with high field methods. *Physics of the Earth and Planetary Interiors*, *82*(2), 113–123. https://doi.org/10.1016/0031-9201(94)90084-1

Rochette, P., Fillion, G., Mattéi, J.-L., & Dekkers, M. J. (1990). Magnetic transition at 30–34 Kelvin in pyrrhotite: Insight into a widespread occurrence of this mineral in rocks. *Earth and Planetary Science Letters*, *98*(3), 319–328. https://doi.org/10.1016/0012-821x(90)90034-u

Rochette, P., Mathé, P. E., Esteban, L., Rakoto, H., Bouchez, J. L., Liu, Q., & Torrent, J. (2005). Non-saturation of the defect moment of goethite and fine-grained hematite up to 57 teslas. *Geophysical Research Letters*, *32*(22). https://doi.org/10.1029/2005gl024196

Schröder, C., Köhler, I., Muller, F. L., Chumakov, A. I., Kupenko, I., Rüffer, R., & Kappler, A. (2016). The biogeochemical iron cycle and astrobiology. *Hyperfine Interactions*, *237*(1), 85. https://doi.org/10.1007/s10751-016-1289-2

Schwertmann, U. (1988). Occurrence and formation of iron oxides in various pedoenvironments. In J. W. Stucki, B. A. Goodman, U. Schwertmann (Eds.) *Iron in soils and clay minerals* (Vol 217, pp. 267–308). *NATO ASI Series (Series C: Mathematical and Physical Sciences)*. Springer, Dordrecht. https://doi.org/10.1007/978-94-009-4007-9_11

Singer, M., Bowen, L., Verosub, K., Fine, P., & TenPas, J. (1995). Mössbauer spectroscopic evidence for citrate-bicarbonate-dithionite extraction of maghemite from soils. *Clays Clay Miner.*, *43*(1), 1–7. https://doi.org/10.1346/ccmn.1995.0430101

Slotznick, S. P., Eiler, J. M., & Fischer, W. W. (2018). The effects of metamorphism on iron mineralogy and the iron speciation redox proxy. *Geochim. Cosmochim. Acta*, *224*, 96–115. https://doi.org/10.1016/j.gca.2017.12.003

Slotznick, S. P., Swanson-Hysell, N. L., & Sperling, E. A. (2018). Oxygenated Mesoproterozoic lake revealed through magnetic mineralogy. *PNAS*, *115*(51), 12938–12943. https://doi.org/10.1073/pnas.1813493115

Slotznick, S. P., Webb, S. M., Kirschvink, J. L., & Fischer, W. W. (2019). Mid-Proterozoic ferruginous conditions reflect postdepositional processes. *Geophysical Research Letters*, *46*(6), 3114–3123. https://doi.org/10.1029/2018gl081496

Slotznick, S. P., Winston, D., Webb, S. M., Kirschvink, J. L., & Fischer, W. W. (2016). Iron mineralogy and redox conditions during deposition of the Mid-Proterozoic Appekunny Formation, Belt Supergroup, Glacier National Park. *Geological Society of America Special Papers*, *522*, 221–242. https://doi.org/10.1130/2016.2522(09)

Slotznick, S. P., Zieg, J., Webb, S. M., Kirschvink, J. L., & Fischer, W. W. (2015). Iron mineralogy and redox chemistry of the Mesoproterozoic Newland Formation in the Helena Embayment, Belt Supergroup, Montana. *Northwest Geology*, *44*, 55–72.

Smit, J., & Wijn, H. (1959). *Ferrites: Physical properties of ferromagnetic oxides in relation to their applications*, 373 pp. Eindhoven, Holland: Philips Technical Library.

Snyder, R., & Bish, D. L. (1989). Quantitative analysis. In D. L. Bish, & J. Post (Eds.), *Reviews in mineralogy and geochemistry*, (pp. 101–144).

Sperling, E. A., Halverson, G. P., Knoll, A. H., Macdonald, F. A., & Johnston, D. T. (2013). A basin redox transect at the dawn of animal life. *Earth and Planetary Science Letters*, *371*, 143–155. https://doi.org/10.1016/j.epsl.2013.04.003

Sperling, E. A., Wolock, C. J., Morgan, A. S., Gill, B. C., Kunzmann, M., Halverson, G. P., et al. (2015). Statistical analysis of iron geochemical data suggests limited late Proterozoic oxygenation. *Nature*, *523*(7561), 451–454. https://doi.org/10.1038/nature14589

Sprain, C. J., Renne, P. R., Clemens, W. A., & Wilson, G. P. (2018). Calibration of chron C29r: New high-precision geochronologic and paleomagnetic constraints from the Hell Creek region, Montana. *GSA Bulletin*, *130*(9-10), 1615–1644. https://doi.org/10.1130/b31890.1

Srodon, J., Drits, V. A., McCarty, D. K., Hsieh, J. C., & Eberl, D. D. (2001). Quantitative X-ray diffraction analysis of clay-bearing rocks from random preparations. *Clays Clay Miner.*, *49*(6), 514–528. https://doi.org/10.1346/ccmn.2001.0490604

Stephenson, A. (1993). Three-axis static alternating field demagnetization of rocks and the identification of natural remanent magnetization, gyroremanent magnetization, and anisotropy. *Journal of Geophysical Research: Solid Earth*, *98*(B1), 373–381. https://doi.org/10.1029/92jb01849

Stookey, L. L. (1970). Ferrozine—A new spectrophotometric reagent for iron. *Analytical Chemistry*, *42*(7), 779–781. https://doi.org/10.1021/ac60289a016

Sun, J., Mailloux, B. J., Chillrud, S. N., van Geen, A., Thompson, A., & Bostick, B. C. (2018). Simultaneously quantifying ferrihydrite and goethite in natural sediments using the method of standard additions with X-ray absorption spectroscopy. *Chem. Geol.*, *476*, 248–259. https://doi.org/10.1016/j.chemgeo.2017.11.021

Sun, W., Banerjee, S. K., & Hunt, C. P. (1995). The role of maghemite in the enhancement of magnetic signal in the Chinese loess-paleosol sequence: An extensive rock magnetic study combined with citrate-bicarbonate-dithionite treatment. *Earth and Planetary Science Letters*, *133*(3-4), 493–505. https://doi.org/10.1016/0012-821x(95)00082-n

Swanson-Hysell, N. L., Fairchild, L. M., & Slotznick, S. P. (2019). Primary and secondary red bed magnetization constrained by fluvial intraclasts. *JGRB*, *124*(5), 4276–4289. https://doi.org/10.1029/2018jb017067

Swanson-Hysell, N. L., Maloof, A. C., Kirschvink, J. L., Evans, D. A., Halverson, G. P., & Hurtgen, M. T. (2012). Constraints on Neoproterozoic paleogeography and Paleozoic orogenesis from paleomagnetic records of the Bitter Springs Formation, Amadeus Basin, central Australia. *Am. J. Sci.*, *312*(8), 817–884. https://doi.org/10.2475/08.2012.01

Tang, D., Shi, X., Jiang, G., Zhou, X., & Shi, Q. (2017). Ferruginous seawater facilitates the transformation of glauconite to chamosite: An example from the Mesoproterozoic Xiamaling Formation of North China. *American Mineralogist: Journal of Earth and Planetary Materials*, *102*(11), 2317–2332. https://doi.org/10.2138/am-2017-6136

Tessier, A., Campbell, P. G., & Bisson, M. (1979). Sequential extraction procedure for the speciation of particulate trace metals. *Analytical Chemistry*, *51*(7), 844–851. https://doi.org/10.1021/ac50043a017

Tikoo, S. M., Weiss, B. P., Buz, J., Lima, E. A., Shea, E. K., Melo, G., & Grove, T. L. (2012). Magnetic fidelity of lunar samples and implications for an ancient core dynamo. *Earth and Planetary Science Letters*, *337*, 93–103. https://doi.org/10.1016/j.epsl.2012.05.024

Till, J., Guyodo, Y., Lagroix, F., Ona-Nguema, G., & Brest, J. (2014). Magnetic comparison of abiogenic and biogenic alteration products of lepidocrocite. *Earth and Planetary Science Letters*, *395*, 149–158. https://doi.org/10.1016/j.epsl.2014.03.051

Trower, E. J., & Fischer, W. W. (2019). Precambrian Si isotope mass balance, weathering, and the significance of the authigenic clay silica sink. *Sediment. Geol.*, *384*, 1–11. https://doi.org/10.1016/j.sedgeo.2019.02.008

Turner, P. (1979). Diagenetic origin of Cambrian marine red beds: Caerfai Bay shales, Dyfed, Wales. *Sediment Geol.*, *24*(3-4), 269–281. https://doi.org/10.1016/0037-0738(79)90073-3

van der Zee, C., Roberts, D. R., Rancourt, D. G., & Slomp, C. P. (2003). Nanogoethite is the dominant reactive oxyhydroxide phase in lake and marine sediments. *Geology*, *31*(11), 993–996. https://doi.org/10.1130/g19924.1

Van Helmond, N. A., Jilbert, T., & Slomp, C. P. (2018). Hypoxia in the Holocene Baltic Sea: Comparing modern versus past intervals using sedimentary trace metals. *Chem. Geol.*, *493*, 478–490. https://doi.org/10.1016/j.chemgeo.2018.06.028

van Houten, F., & Purucker, M. (1984). Glauconitic peloids and chamositic ooids-favorable factors, constraints, and problems. *Earth-Sci. Rev.*, *20*(3), 211–243. https://doi.org/10.1016/0012-8252(84)90002-3

van Oorschot, I. H. M. (2001). Chemical distinction between lithogenic and pedogenic iron oxides in environmental magnetism: A search for the perfect solution. *Geologica Ultraiectina* (Vol. 208, pp. 199). *(Doctoral dissertation)*. Utrecht University. https://dspace.library.uu.nl/bitstream/handle/1874/542/full.pdf

van Oorschot, I. H. M., & Dekkers, M. (1999). Dissolution behaviour of fine-grained magnetite and maghemite in the citrate–bicarbonate–dithionite extraction method. *Earth and Planetary Science Letters*, *167*(3-4), 283–295. https://doi.org/10.1016/s0012-821x(99)00033-3

van Oorschot, I. H. M., Grygar, T., & Dekkers, M. (2001). Detection of low concentrations of fine-grained iron oxides by voltammetry of microparticles. *Earth and Planetary Science Letters*, *193*(3-4), 631–642. https://doi.org/10.1016/s0012-821x(01)00502-7

Velde, B., Raoult, J.-F., & Leikine, M. (1974). Metamorphosed berthierine pellets in mid-Cretaceous rocks from north-eastern Algeria. *Journal of Sedimentary Research*, *44*(4), 1275–1280. https://doi.org/10.1306/212f6c99-2b24-11d7-8648000102c1865d

Verwey, E. (1939). Electronic conduction of magnetite (Fe_3O_4) and its transition point at low temperatures. *Nature*, *144*(3642), 327–328. https://doi.org/10.1038/144327b0

von der Heyden, B. P., Frith, M. G., Bernasek, S., Tylizszak, T., Roychoudhury, A. N., & Myneni, S. C. (2018). Geochemistry of Al and Fe in freshwater and coastal water colloids from the west coast of Southern Africa. *Geochim. Cosmochim. Acta*, *241*, 56–68. https://doi.org/10.1016/j.gca.2018.08.043

Walker, T. R., Larson, E. E., & Hoblitt, R. P. (1981). Nature and origin of hematite in the Moenkopi Formation (Triassic), Colorado Plateau: A contribution to the origin of magnetism in red beds. *Journal of Geophysical Research*, *86*(B1), 317–333. https://doi.org/10.1029/jb086ib01p00317

Wang, J., Aguilar, V., Li, L., Li, F.-g., Wang, W.-z., & Zhao, G.-m. (2015). Strong shape-dependence of Morin transition in α-Fe_2O_3 single-crystalline nanostructures. *Nano Research*, *8*(6), 1906–1916. https://doi.org/10.1007/s12274-014-0700-z

Wang, X., Zhu, M., Koopal, L. K., Li, W., Xu, W., Liu, F., et al. (2016). Effects of crystallite size on the structure and magnetism of ferrihydrite. *Environmental Science: Nano*, *3*(1), 190–202. https://doi.org/10.1039/c5en00191a

Weil, A. B., & Van der Voo, R. (2002). Insights into the mechanism for orogen-related carbonate remagnetization from growth of authigenic Fe-oxide: A scanning electron microscopy and rock magnetic study of Devonian carbonates from northern Spain. *Journal of Geophysical Research: Solid Earth*, *107*(B4). https://doi.org/10.1029/2001jb000200

Yamazaki, T., & Solheid, P. (2011). Maghemite-to-magnetite reduction across the Fe-redox boundary in a sediment core from the Ontong-Java Plateau: Influence on relative palaeointensity estimation and environmental magnetic application. *Geophysical Journal International*, *185*(3), 1243–1254. https://doi.org/10.1111/j.1365-246x.2011.05021.x

Zergenyi, R., Hirt, A., Zimmermann, S., Dobson, J., & Lowrie, W. (2000). Low-temperature magnetic behavior of ferrihydrite. *Journal of Geophysical Research: Solid Earth*, *105*(B4), 8297–8303. https://doi.org/10.1029/1999jb900315